CHALMERS
UNIVERSITY OF TECHNOLOGY

UNIVERSITY OF GOTHENBURG

Survey on Seamless On-Board and Cloud Connectivity for Transport Missions

Master's thesis in Electrical engineering

UZAIR MUHAMMAD

Department of Electrical Engineering
CHALMERS UNIVERSITY OF TECHNOLOGY
UNIVERSITY OF GOTHENBURG
Gothenburg, Sweden 2025

Master's thesis 2025

Survey on Seamless On-Board and Cloud Connectivity for Transport Missions

UZAIR MUHAMMAD

UNIVERSITY OF
GOTHENBURG

CHALMERS
UNIVERSITY OF TECHNOLOGY

Department of Electrical Engineering
Chalmers University of Technology
University of Gothenburg
Gothenburg, Sweden 2025

Survey on Seamless On-Board and Cloud Connectivity for Transport Missions

UZAIR MUHAMMAD

Advisor: Homa Taherisefat, Department of Electrical Engineering
Supervisor: José Vilca, Yasaman Ettefagh, Volvo Group
Examiner: Henk Wymeersch, Department of Electrical Engineering

Master's Thesis 2025
Department of Electrical Engineering
Chalmers University of Technology and University of Gothenburg
SE-412 96 Gothenburg
Telephone +46 31 772 1000

Typeset in LaTeX
Gothenburg, Sweden 2025

Survey on Seamless On-Board and Cloud Connectivity for Transport Missions

UZAIR MUHAMMAD
Department of Electrical Engineering
Chalmers University of Technology and University of Gothenburg

Abstract

The reliable connectivity required for mission-critical transport systems, such as autonomous driving, remains a challenge in areas with limited terrestrial network coverage. Non-Terrestrial Networks (NTNs), particularly Low Earth Orbit (LEO) satellites, have emerged as a promising solution to fill this gap.

The study employs a comprehensive MATLAB-based simulation framework informed by 3GPP TR 38.811 and ITU-R channel models. The methodology involves a systematic approach where free-space path loss, atmospheric attenuation, Doppler shift, and environmental fading are integrated into a complete link budget. The primary contribution of this research is its integrated analysis of these factors specifically for vehicular links, providing a unified assessment of performance through key metrics including Bit Error Rate (BER) versus Carrier-to-Noise Ratio (CNR), BER versus E_b/N_0, throughput, latency, and Doppler shift.

The results demonstrate that elevation angle is the dominant factor governing link quality. Performance improves dramatically from near-unusable conditions at 10° to reliable, near-error-free operation (BER $< 10^{-6}$) at 90° elevation. A critical finding is the establishment of a universal CNR threshold of approximately 15 dB for reliable operation. The analysis reveals a fundamental design trade-off: Ka-band offers higher throughput, while S-band provides robustness against impairments. Latency analysis confirms that LEO systems can meet the delay requirements for connected transport services.

This study concludes that LEO-based NTNs are a viable complementary technology for intelligent transportation systems. The findings provide a clear framework for system design, highlighting the critical importance of elevation-aware planning and strategic frequency band selection.

Keywords: Non-Terrestrial Networks (NTNs), Low Earth Orbit (LEO) Satellites, Autonomous Transport, Satellite Communication, Elevation Angle, Frequency Bands, Path Loss, Atmospheric Attenuation, Latency, Doppler Effects, Physical-Layer Simulation, 3GPP Channel Models.

Acknowledgements

First and foremost, I sincerely thank my industry supervisor at Volvo Group, **José Vilca** and **Yasaman Ettefagh**, for their valuable guidance, technical insights, and continuous support during this project. Their expertise and encouragement provided a strong foundation for connecting academic research with real-world applications and significantly contributed to the depth of this work.

I am also deeply grateful to my academic advisors, **Homa Taherisefat**, from the Department of Electrical Engineering, for her continuous guidance, constructive feedback, and encouragement. Her support was instrumental in navigating the academic aspects of the thesis and maintaining a clear research direction.

Uzair Muhammad, Gothenburg, 2025-11-26

Declaration on the Use of AI Tools

AI-assisted tools (e.g., ChatGPT) were used only for grammar/readability.All technical content, code, analyses, and conclusions are the author's own.

Abbreviations

NTN	Non-Terrestrial Network
LEO	Low Earth Orbit
GEO	Geostationary Earth Orbit
MEO	Medium Earth Orbit
HAPS	High-Altitude Platform Station
AD/ADAS	Autonomous Driving / Advanced Driver Assistance Systems
UE	User Equipment
OFDM	Orthogonal Frequency Division Multiplexing
QPSK	Quadrature Phase Shift Keying
QAM	Quadrature Amplitude Modulation
FSPL	Free-Space Path Loss
CL	Clutter Loss
SF	Shadow Fading
SNR	Signal-to-Noise Ratio
CNR	Carrier-to-Noise Ratio
BER	Bit Error Rate
QoS	Quality of Service
CF	Carrier Frequency
ITU	International Telecommunication Union
3GPP	3rd Generation Partnership Project
eMBB	enhanced Mobile Broadband
URLLC	Ultra-Reliable Low Latency Communication
mMTC	massive Machine-Type Communication
KPIs	Key Performance Indicators

SDR	Software-Defined Radio
LoS	Line of Sight
C-RAN	Centralized Radio Access Network
ISI	inter-symbol interference
MSS	Mobile Satellite Service
NR	New Radio
RF	Radio Frequency

Contents

List of Figures

List of Tables

1

Introduction

In recent years, advancements in Autonomous Driving / Advanced Driver Assistance Systems (AD/ADAS) have accelerated the transformation of the transportation industry. These technologies promise enhanced road safety, reduced human error, and greater efficiency in transport missions. However, their deployment heavily depends on seamless onboard and cloud connectivity to meet the significant computational demands of distributed multi-agent systems. Traditional processing and communication solutions are constrained by the physical space and limited electrical capacity available in vehicles, making them insufficient for future autonomous operations [1].

Non-Terrestrial Network (NTN)s, including Low Earth Orbit (LEO) satellites and High-Altitude Platform Station (HAPS), have emerged as a promising solution. They offer robust, scalable, and globally available connectivity with lower latency and higher throughput compared to traditional terrestrial systems [2]. This thesis explores the integration of NTNs into vehicular networks to support mission-critical operations, with a focus on enhancing the cloud connectivity required for autonomous transport systems.

1.1 Literature Review and Research Gap

1.1.1 Non-Terrestrial Networks in 5G and Beyond

NTNs have become an essential component of 3GPP's vision for enhanced 5G and future 6G systems. The importance of LEO mega-constellations in achieving global broadband access with lower latency and improved link reliability has been extensively documented in recent literature [3], [4]. These studies provide comprehensive overviews of NTN architectures and identify LEO systems as key enablers for scalable and resilient connectivity, while emphasizing the significant opportunities opened by satellite-terrestrial integration in future 6G networks.

Standardization efforts by 3GPP documented in TR 38.811 and TR 38.821 define channel models, deployment scenarios, and performance requirements for NR-based NTN communication [5]. These technical reports establish the foundation for satellite-supported 5G services and identify challenges such as long propagation distances, high Doppler variation, and atmospheric impairments.

1.1.2 LEO Satellite Communication Performance

LEO satellites provide reduced propagation delay compared to traditional GEO systems due to their lower orbital altitude, making them suitable for latency-sensitive applications. Doppler effects in LEO networks have been extensively studied, revealing that high orbital velocity introduces substantial frequency shifts that must be mitigated for reliable communication [6]. Similarly, waveform performance and synchronization challenges have been assessed, with research identifying OFDM as a robust candidate when paired with appropriate compensation techniques [7].

Propagation impairments also significantly affect LEO communication, particularly rain attenuation at Ka-band frequencies where weather-induced fading is more pronounced at higher frequencies [8]. Studies on link budget and constellation design further highlight elevation angle as a major factor influencing path loss, CNR, and link availability [9].

These works collectively provide essential insights into the physical-layer behavior of LEO systems but do not specifically analyze their performance in autonomous vehicular contexts.

1.1.3 NTN for Vehicular and V2X Communication

The integration of satellite communication into V2X systems has recently gained momentum. Satellite-aided vehicular communication has been explored, discussing the potential for extending connectivity in areas where terrestrial networks fall short [10]. Hybrid satellite-terrestrial V2X architectures have been evaluated, highlighting the potential of LEO systems to support safety-critical vehicular applications [11].

Further studies examine the feasibility of satellite communication for vehicular broadband and identify key factors—including elevation angle and shadowing—that affect link performance [12]. However, existing research often relies on simplified link assumptions and lacks a detailed physical-layer analysis aligned with 3GPP NTN models.

1.1.4 Communication Requirements for AD/ADAS

Autonomous and connected vehicles require ultra-reliable and low-latency communication to support cooperative perception, distributed decision-making, and real-time sensor sharing. Research indicates that many autonomous driving functions require under 10 ms end-to-end latency and extremely high reliability [13]. Similar demands have been identified, emphasizing the importance of consistent connectivity for safety-related functions [14]. Industry-driven analyses highlight the need for seamless coverage even in rural or infrastructure-limited environments [15].

Current studies predominantly assume terrestrial 5G availability and do not evaluate the feasibility of satellite links for meeting AD/ADAS communication demands.

1.1.5 Synthesis and Research Direction

The reviewed literature establishes a strong foundation in NTN architectures, LEO satellite performance characteristics, and vehicular communication requirements. However, the intersection of these domains—specifically evaluating LEO NTN performance against rigorous AD/ADAS connectivity requirements using standardized 3GPP channel models—remains underexplored. This gap motivates the systematic evaluation approach adopted in this thesis.

1.1.6 Identified Research Gap

Although research on NTN systems, satellite channel models, and hybrid V2X communication has progressed in recent years, several important gaps remain. Many existing studies do not evaluate how well LEO satellite links meet the specific communication requirements of AD/ADAS applications, such as latency, reliability, and throughput. In addition, a large part of the literature relies on simplified channel assumptions and does not consider detailed physical-layer behavior under 3GPP-compliant NTN models, including metrics like BER, CNR, and E_b/N_0.

Another limitation is that the effects of elevation angle, Doppler shift, and different environmental conditions are often studied separately, rather than in a combined and systematic way that reflects realistic vehicular communication scenarios. Furthermore, few works connect satellite channel characteristics directly with the needs of autonomous transport systems, which makes it difficult to assess the practical suitability of NTN for mission-critical mobility services.

1.2 Aim

This thesis aims to survey and evaluate the feasibility of using NTNs for providing seamless, mission-critical onboard and cloud connectivity to support transport missions involving vehicles such as cars and trucks. It defines the necessary Quality of Service (QoS) requirements for reliable AD/ADAS operations and investigates the ability of NTNs to fulfill these requirements through literature review and MATLAB-based channel model simulations.

1.3 Research Questions

- **Primary Research Question:**
  How can NTN ensure seamless connectivity and meet the requirements of mission-critical transport systems?
- **Sub-Questions:**
  - What are the minimum connectivity quality requirements (e.g., latency, throughput, reliability) necessary for robust AD/ADAS operations?
  - How can NTNs address the limitations of terrestrial-based connectivity in transport missions?

1.4 Limitations

This thesis primarily focuses on the communication and channel modeling aspects of establishing connectivity between vehicles and the cloud via NTNs, with particular emphasis on LEO satellites. The study does not explore the detailed architecture of vehicle-side computational systems nor propose satellite hardware designs. Instead, it concentrates on evaluating the feasibility and performance of NTN-based vehicular communication through simulation models informed by 3GPP technical reports and established literature.

2

Theoretical Background

The deployment of NTNs to support vehicular communication systems requires a comprehensive understanding of wireless transmission principles, satellite communication fundamentals, and signal processing techniques. This chapter provides the theoretical framework necessary to model and evaluate NTN-based connectivity solutions for transport missions, progressing systematically from fundamental concepts to practical application scenarios.

The discussion begins with wireless communication fundamentals, covering the basic principles of electromagnetic signal propagation, and introducing Orthogonal Frequency Division Multiplexing (OFDM) as the cornerstone transmission scheme in modern 5G networks [16]. Building upon this foundation, the chapter explores non-terrestrial network architectures, focusing on satellite communication systems with emphasis on LEO constellations, detailing transparent and regenerative payload architectures and their relevance to vehicular use cases as defined in 3GPP standards [5].

The analysis then moves to wireless channel modeling, examining key impairments affecting satellite-to-vehicle links including free-space path loss, atmospheric attenuation, Doppler effects caused by satellite motion, shadow fading due to signal obstruction, and clutter loss from environmental scattering. These channel effects are then examined through practical application scenarios including rural areas, dense urban centers, and remote regions, demonstrating how each environment presents unique challenges for NTN integration in transport missions. Finally, the chapter establishes performance evaluation metrics that provide the quantitative framework for assessing communication quality, covering Bit Error Rate (BER), Carrier-to-Noise Ratio (CNR), E_b/N_0, latency, doppler shift and throughput metrics essential for vehicular applications.

2.1 Wireless Communication Fundamentals

Wireless communication enables the transmission of information over distances without the need for physical connections such as wires or optical fibers. Information is carried by electromagnetic waves, which propagate through space and interact with the environment. Key properties such as signal characteristics, propagation behavior, modulation techniques, path loss, and doppler shift play a critical role

in the design and performance analysis of modern wireless communication systems [16].

2.1.1 Wireless Signal Characteristics

A wireless signal is typically a modulated electromagnetic wave used to convey information through free space. Its behavior is governed by several fundamental wave properties, illustrated in Fig. 2.1.

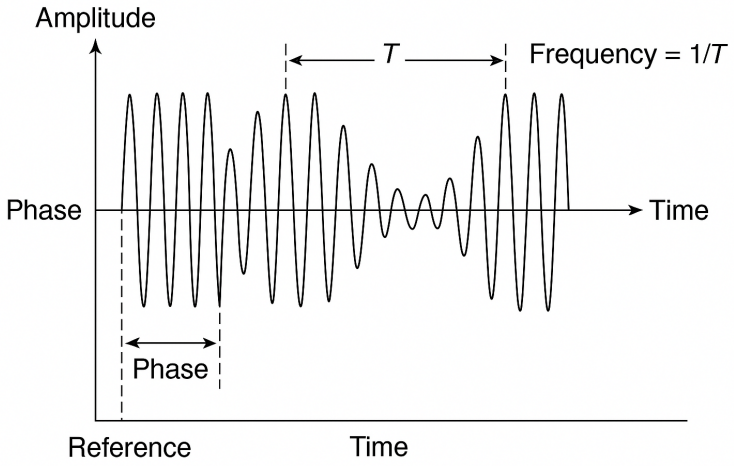

Figure 2.1: Wireless signal characteristics [17].

The essential physical characteristics of a wireless signal include frequency, wavelength, amplitude, and phase. The frequency (f), measured in Hertz (Hz), determines how many oscillations occur per second and influences propagation behavior and spectrum allocation. Wavelength (λ) is the spatial distance between two successive wave peaks and is related to frequency by $\lambda = c/f$, where c is the speed of light; this relationship affects antenna design, diffraction, and path loss. Amplitude reflects the signal strength or power (commonly measured in dBm or Watts), and variations in amplitude form the basis for amplitude-based modulation schemes. Phase describes the position of the waveform relative to a time reference, measured in degrees or radians, and is critical for coherent modulation and synchronization in modern communication systems.

Beyond these intrinsic wave properties, several system-level parameters determine communication performance. Bandwidth (B), measured in Hz, defines the frequency span occupied by the signal and directly influences the maximum achievable data rate according to Shannon's capacity limit,

$$C = B \log_2(1 + \mathrm{SNR})[18].$$

The data rate, expressed in $\mathrm{bit\,s^{-1}}$, depends on the available bandwidth, modulation order, and coding rate. Delay in wireless communication consists of multiple components: propagation delay caused by the finite speed of electromagnetic waves,

processing delay from modulation, encoding, and baseband operations, and queuing delay stemming from network buffers during congestion. The total latency is the end-to-end sum of these delays and is especially important for real-time applications such as autonomous vehicle control.

Together, these properties determine how wireless signals propagate, how much information they can carry, and the overall quality of service achievable in communication systems [16].

2.1.2 Wireless Signal Propagation Mechanisms

As wireless signals travel through space and Earth's atmosphere in NTN systems, they are affected by various physical phenomena including free-space path loss, atmospheric effects, and terrestrial interactions that collectively influence communication quality and reliability [19], [20].

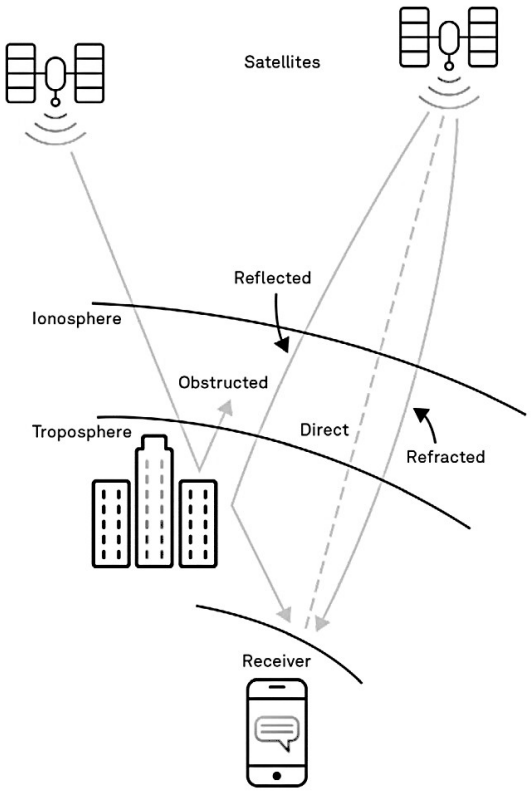

Figure 2.2: Signal propagation effects in satellite communications [21].

These effects are particularly important in NTNs, where the signal path between satellite and ground terminals traverses multiple propagation regimes: vacuum of space, various atmospheric layers, and complex terrestrial environments.

- **Free-Space Propagation:** In the vacuum of space, signals follow the free-space path loss model where received power decreases with the square of the

distance. For LEO satellite links, this is the dominant effect during most of the 500 km to 2000 km path between satellite and ground terminal.

- **Atmospheric Effects:** As signals penetrate Earth's atmosphere, they encounter several impairments. Gaseous absorption from oxygen and water vapor causes frequency-dependent attenuation, particularly above 10 GHz. Rain attenuation becomes significant at Ka-band and higher frequencies, with rainfall rates directly impacting link availability. Cloud and fog attenuation affects higher frequencies, while ionospheric effects including scintillation and Faraday rotation impact lower frequency bands [20], [22].

- **Reflection:** When NTN signals approach Earth's surface, they may reflect off large surfaces such as water bodies, buildings, or vehicles [23]. Reflections cause constructive or destructive interference, leading to signal fading or multipath distortion that is particularly challenging in urban environments with low elevation satellite links.

- **Diffraction:** In scenarios where direct line-of-sight is obstructed by terrain or urban structures, signals diffract around obstacles. While diffraction helps maintain connectivity, it results in significant signal attenuation that affects NTN link reliability, especially at low elevation angles where the signal path intersects more obstacles.

- **Scattering:** Small-scale obstacles including foliage, vehicles, and rough surfaces cause signal scattering in multiple directions. In NTN-based vehicular communication, scattering becomes prominent in both rural and urban environments, reducing signal coherence and increasing bit error rates under mobility conditions.

These propagation effects become more pronounced in NTN systems operating at higher frequencies (e.g., Ka-band), where atmospheric losses and signal distortions significantly impact link budget calculations and system availability [20], [24].

2.1.3 OFDM in Modern Wireless Systems

OFDM is a popular technique employed in modern wireless standards, including LTE and 5G [25]. In OFDM, the available bandwidth is divided into multiple closely spaced orthogonal subcarriers, each carrying a low-rate data stream. This improves robustness against multipath fading and simplifies equalization at the receiver [26].

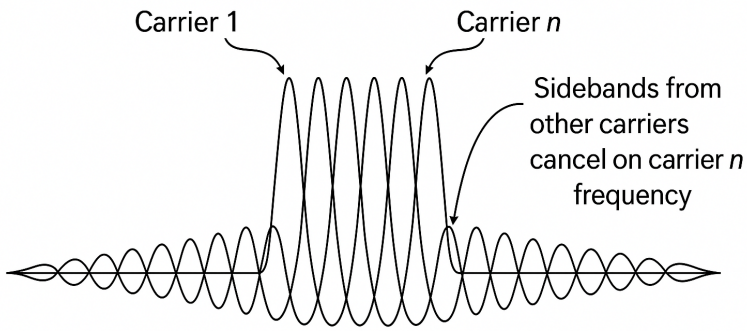

Figure 2.3: Basic OFDM concept [27].

The OFDM signal in the time domain can be mathematically expressed as [28]:

$$s(t) = \sum_{k=0}^{N-1} X_k e^{j2\pi f_k t} \tag{2.1}$$

Where X_k is the complex data symbol mapped to the k-th subcarrier, f_k is the frequency of the k-th subcarrier, and N is the total number of subcarriers.

The orthogonality between subcarriers ensures that they do not interfere with each other despite their close spectral spacing. This enables high spectral efficiency and simplified receiver design using Fast Fourier Transform (FFT) techniques.

In the context of this thesis, OFDM is used as the base waveform for evaluating the physical layer performance of satellite communication links, particularly in dynamic scenarios such as vehicular mobility and varying elevation angles.

2.1.4 Noise in Wireless Systems

Wireless signals are always affected by noise, which degrades communication quality and limits system performance. The widely used Additive White Gaussian Noise (AWGN) model characterizes this phenomenon through three key properties: additive (noise superimposed on the signal), white (constant power spectral density across frequencies), and Gaussian (noise amplitude following a normal distribution) [16].

AWGN establishes a fundamental limit on the minimum signal strength required for reliable communication and serves as a baseline for analyzing and designing communication systems.

2.2 Satellite Communication

Satellite communication systems provide wireless connectivity by utilizing spacecraft as relay stations between Earth-based users and network gateways. These systems enable services such as television broadcasting, global navigation, remote sensing,

and increasingly, broadband internet access [19], [23]. The fundamental design of a satellite network is influenced by the satellite's orbital characteristics, which determine coverage area, signal delay, and communication performance.

Satellites generally operate in one of three main types of orbits: LEO, Medium Earth Orbit (MEO), and Geostationary Earth Orbit (GEO) . Each orbit offers distinct advantages and is suited for specific applications.

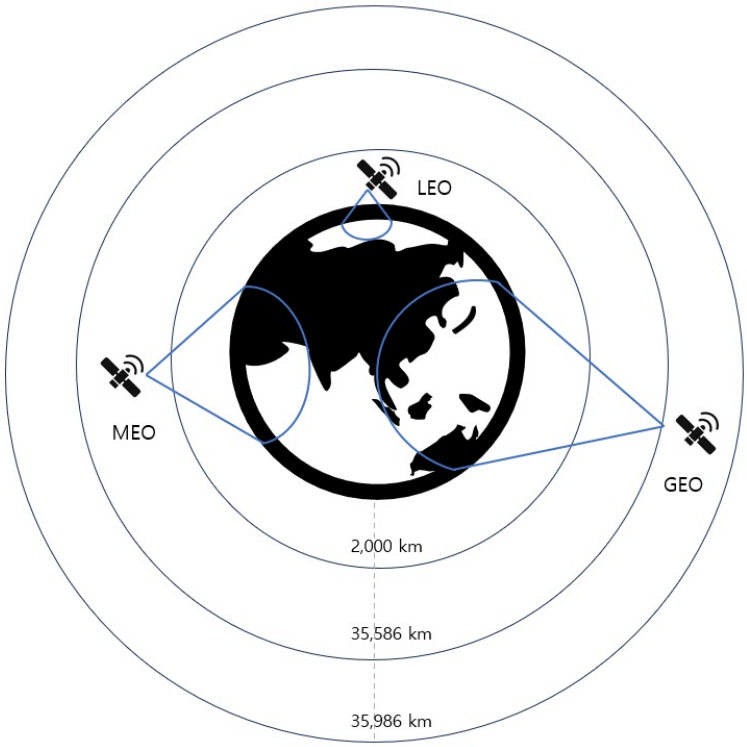

Figure 2.4: Satellite orbit classification: relative to Earth [29].

Figure 2.4 illustrates the relative altitudes and coverage areas of LEO, MEO, and GEO satellites. LEO satellites orbit closest to the Earth, providing low-latency links but requiring a larger number of satellites to achieve continuous global coverage. MEO satellites orbit at intermediate altitudes, balancing coverage and latency. GEO satellites, positioned at approximately 35,786 km altitude, maintain a fixed position relative to the Earth's surface, offering broad coverage with higher transmission delays [23].

With the evolution of wireless networks towards 5G and beyond, satellites are playing an increasingly critical role in building Non-Terrestrial Networks [24]. NTNs aim to extend terrestrial mobile networks by providing connectivity in underserved and remote regions, supporting continuous communication for vehicles, ships, aircraft, and IoT devices. LEO constellations, in particular, offer significant potential for NTN integration due to their low-latency characteristics, which align with the stringent requirements of 5G and future 6G services [5].

To better understand the differences among orbital types, Table 2.1 summarize key parameters such as altitude, orbital period, communication delay, and velocity.

Table 2.1: Satellite orbit characteristics

Orbit Type	**Altitude** (km)	**Orbital Period**	**Delay** (ms)	**Velocity** ($\mathrm{km\,s^{-1}}$)
LEO	500–2,000	90–120 min	5–25	7.5
MEO	2,000–20,000	2–12 hrs	50–150	3.0–5.5
GEO	35,786	24 hrs (stationary)	250–600	3.07

Each orbit type presents unique challenges:

- **LEO**: Although offering low latency, LEO networks require dense constellations and complex handover mechanisms due to the high velocity and frequent satellite transitions.
- **MEO**: MEO systems strike a balance between coverage and latency but suffer from moderate delay, making them suitable for navigation services (e.g., GPS) rather than ultra-low-latency applications.
- **GEO**: GEO satellites offer extensive coverage with minimal ground infrastructure but suffer from high propagation delays and signal attenuation, limiting their use for latency-sensitive services.

2.2.1 5G Non-Terrestrial Networks and Architecture Principles

5G NTNs extend the traditional terrestrial cellular infrastructure by incorporating satellites and aerial platforms into the network architecture. It aims to provide global coverage, support mobility across remote and under-served areas, and enhance the resilience of communication networks for mission-critical applications.

The standardization of NTNs within the 5G framework has been driven primarily by the 3rd Generation Partnership Project (3GPP), particularly in documents such as TR 38.811 and TR 38.821. These technical reports outline the architectural principles, deployment scenarios, and channel models necessary for integrating satellite systems into 5G New Radio (NR) networks.

2.2.2 Deployment Architectures

There are two main types of satellite payload architectures defined [5]:

- **Transparent Payload (Bent-Pipe Architecture):** In a transparent payload, the satellite simply acts as a relay between the User Equipment (UE) and the terrestrial gateway. The signal is transmitted without any processing done on satellite. All control and data management operations are performed at the gateway. This approach benefits from reduced satellite complexity and cost but may suffer from higher latency and limited flexibility in resource management [5].
- **Regenerative Payload (Onboard Processing Architecture):** In a regenerative payload, the satellite performs signal processing functions onboard, such as demodulation, decoding, and routing. Only the processed data is forwarded

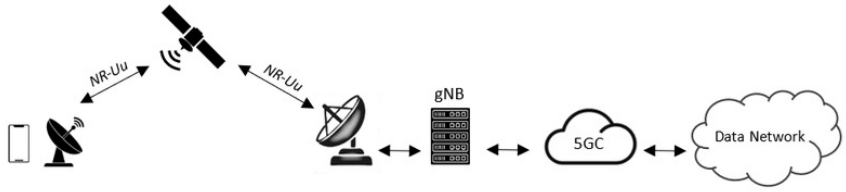

Figure 2.5: 5G NTN transparent mode [5].

to the gateway. This enables lower end-to-end latency, better link adaptation, and improved spectral efficiency, at the cost of increased satellite complexity, size, and power requirements [5].

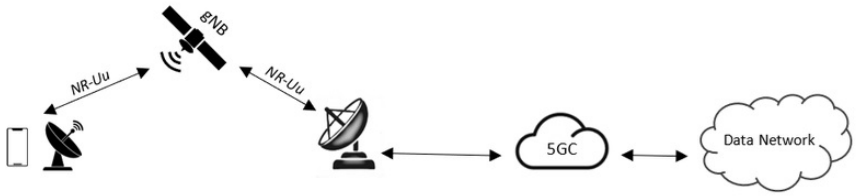

Figure 2.6: 5G NTN regenerative mode [5].

The integration of NTNs into 5G and future 6G ecosystems is expected to significantly enhance global connectivity and enable new applications and services.

2.3 Channel Modeling for NTN Systems

2.3.1 Free-Space Path Loss

In Non-Terrestrial Networks, the Free-Space Path Loss (FSPL) quantifies the attenuation of a radio signal as it propagates through free space without obstruction. It primarily depends on the slant range (d) between the satellite and the ground terminal and the carrier frequency (f) of the transmitted signal.

According to the 3GPP TR 38.811 model, FSPL in decibels is given by [5]:

$$\text{FSPL (dB)} = 20\log_{10}(d) + 20\log_{10}(f) + 32.45 \tag{2.2}$$

where d represents the slant range between the satellite and receiver expressed in metres (m), and f denotes the carrier frequency expressed in GHz. The constant 32.45 originates from the Friis transmission equation and remains valid here for consistency with the 3GPP formulation, ensuring direct comparability with results and reference values defined in 3GPP TR 38.811.

The slant range is the geometric distance between a satellite in orbit and a ground terminal at a specific elevation angle. It varies with both the satellite's altitude and the user's elevation angle, and is calculated using the following expression derived from orbital geometry [5]:

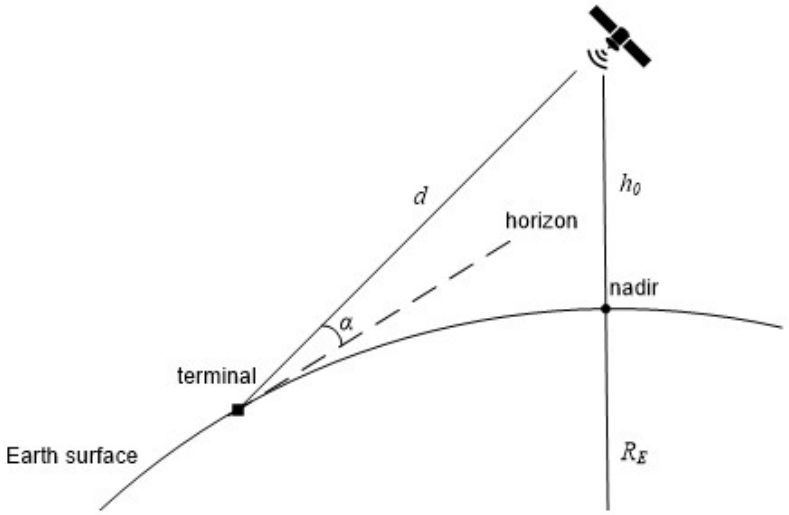

Figure 2.7: Geometry of slant range [5]

$$d = \sqrt{R_E^2 \cdot \sin^2(\alpha) + h^2 + 2hR_E} - R_E \cdot \sin(\alpha) \tag{2.3}$$

In this formulation, R_E represents Earth's radius with a typical value of 6371 km, h denotes the satellite altitude in metres, and α is the elevation angle measured in degrees. This geometric relationship accounts for the spherical Earth geometry and enables accurate calculation of propagation path length for various satellite positions and ground terminal locations.

2.3.2 Large-Scale Path Loss Modeling for NTN Systems

While free-space path loss provides the fundamental propagation attenuation in satellite communications, practical NTN deployments must account for environmental factors that significantly impact link performance. In terrestrial and near-terrestrial environments, additional large-scale impairments become critical for accurate channel modeling [5], [30].

Two primary environmental factors dominate large-scale path loss variations in NTN scenarios:

Clutter Loss (CL) represents signal attenuation caused by obstructions in proximity to the user terminal, including buildings, vegetation, and terrain features. This loss component accounts for the additional attenuation when the signal path intersects physical objects near the receiver location [31].

Shadow Fading (SF) models the large-scale signal fluctuation resulting from obstruction of the line-of-sight path by major obstacles such as buildings, hills, or dense vegetation. Shadow fading is typically modeled as a log-normal distribution with environment-dependent standard deviation, representing the statistical variation of signal strength around the mean path loss [32].

To accurately reflect realistic propagation conditions in NTN deployments, a composite path loss metric is employed that integrates both fundamental and environmental components [5]:

$$\mathrm{PL}_{\mathrm{total}} = \mathrm{FSPL} + \mathrm{CL} + \mathrm{SF} \tag{2.4}$$

where FSPL represents the free-space path loss calculated from satellite geometry, CL denotes the clutter loss specific to the local environment, and SF accounts for shadow fading variations.

Environment-Specific Characteristics

Different deployment environments exhibit distinct propagation characteristics that must be accounted for in NTN system design:

Rural Environments are characterized by natural terrain features and vegetation, where clutter loss primarily results from foliage attenuation and gentle terrain variations. Shadow fading variations are typically moderate due to the relatively open nature of these environments [32].

Urban Environments introduce building penetration losses and street canyon effects, where signals experience multiple reflections and diffractions. The intermediate building density results in moderate additional losses compared to rural scenarios [33].

Dense Urban Environments present the most challenging propagation conditions with severe multipath propagation, deep shadowing effects from tall buildings, and significant building penetration losses. These environments exhibit the highest cumulative additional losses due to the complex urban morphology [31].

The standard deviation of shadow fading typically ranges from 4 dB in open rural areas to 8 dB or more in dense urban environments, reflecting the increasing variability of signal strength in complex propagation scenarios [32].

2.3.3 Atmospheric Effects

In satellite communication, signals transmitted from space to Earth must propagate through the Earth's atmosphere. During this journey, various atmospheric layers introduce impairments, particularly at higher frequencies. These atmospheric effects contribute to signal attenuation, which impacts link budget and system performance.

The main atmospheric effects include [20]:

- **Gaseous absorption** (primarily due to oxygen and water vapor),
- **Rain attenuation**
- **Scintillation** (rapid fluctuations due to tropospheric turbulence),
- **Cloud and fog attenuation**.

Total Atmospheric Attenuation

The total atmospheric loss L_{atm} (in dB) can be expressed as the sum of individual components [20]:

$$L_{\text{atm}} = L_{\text{gas}} + L_{\text{rain}} + L_{\text{cloud}} + L_{\text{scint}} \tag{2.5}$$

However, in many practical models (e.g., ITU-R P.676 for gases, ITU-R P.838 for rain), only the gaseous and rain attenuation are included due to their dominant effect.

Gaseous Absorption

Attenuation due to oxygen and water vapor increases with frequency and is more prominent above 10 GHz. It is calculated using [22]:

$$L_{\text{gas}}(f, h, \alpha) = \gamma_{\text{gas}}(f, h) \cdot \sec(\alpha) \tag{2.6}$$

where:

- γ_{gas} is the specific attenuation [dB km^{-1}],
- h is the altitude of the station,
- α is the elevation angle,
- $\sec(\alpha)$ accounts for slant path length through the atmosphere.

Rain Attenuation

Rain-induced attenuation becomes significant at frequencies above 10 GHz.It depends on rainfall rate R [mm/h] and is modeled as [34]:

$$L_{\text{rain}} = \gamma_R \cdot d_{\text{eff}} \tag{2.7}$$

where:

- $\gamma_R = kR^{\alpha}$ is the specific rain attenuation [dB km^{-1}],
- k and α are frequency-dependent coefficients from ITU-R P.838,
- d_{eff} is the effective path length through the rain [km].

Note: In clear-sky conditions, $L_{\text{rain}} \approx 0$. In simulations based on 3GPP TR 38.811, clear-sky conditions are often assumed unless otherwise stated.

Frequency Dependency

Atmospheric attenuation increases significantly with carrier frequency. For example:

- At **S-band** (2 GHz): $L_{\text{atm}} < 0.5$ dB for most elevation angles,
- At **Ka-band** (20 GHz): L_{atm} can exceed 2 –3 dB even under clear-sky.

This is aligned with observed values in simulation where:

- For S-band: AtmosphericLoss $\approx 0.07\,\mathrm{dB}$ at zenith.
- For Ka-band: AtmosphericLoss $\approx 1.5\,\mathrm{dB}$ or more depending on elevation angle [5].

Elevation Angle Consideration

Since the signal travels a longer path through the atmosphere at low elevation angles, atmospheric losses are higher near the horizon and reduce toward zenith [20]:

$$L_{\mathrm{atm}}(\alpha) \propto \frac{1}{\sin(\alpha)} \tag{2.8}$$

Impact on Link Budget

Atmospheric losses are included in the total path loss as a fundamental component of the link budget [23]:

$$L_{\mathrm{total}} = L_{\mathrm{FSPL}} + L_{\mathrm{atm}} \tag{2.9}$$

which directly affects received power, CNR, Signal-to-Noise Ratio (SNR), and thus, BER and throughput.

2.3.4 Doppler Effect

The Doppler effect refers to the change in frequency observed due to the relative motion between the transmitter and receiver. In the context of LEO satellite communication, this phenomenon becomes significant due to the high orbital speed of satellites and must be accounted for, particularly at higher carrier frequencies.

Basic Doppler Effect Expression

The instantaneous Doppler frequency shift observed at the receiver is given by [24]:

$$f_d = \frac{v_r}{c} \cdot f_c \tag{2.10}$$

where f_d represents the Doppler frequency shift in Hz, v_r is the radial line-of-sight velocity between satellite and receiver in $\mathrm{m\,s^{-1}}$, f_c denotes the carrier frequency in Hz, and $c \approx 3 \times 10^8\ \mathrm{m\,s^{-1}}$ is the speed of light.

Satellite Orbital Velocity

For a satellite in a circular orbit, the orbital velocity v_s is calculated as [24]:

$$v_s = \sqrt{\frac{G \cdot M_e}{R_e + h}} \tag{2.11}$$

with gravitational constant $G = 6.674 \times 10^{-11}\,\mathrm{m^3\,kg^{-1}\,s^{-2}}$, Earth's mass $M_e = 5.972 \times 10^{24}\,\mathrm{kg}$, Earth's radius $R_e = 6.371 \times 10^6\,\mathrm{m}$, and satellite altitude h above Earth in m.

For a typical LEO altitude of $h = 600\,\text{km}$:

$$v_s = \sqrt{\frac{6.674 \times 10^{-11}\,\text{m}^3\,\text{kg}^{-1}\,\text{s}^{-2} \cdot 5.972 \times 10^{24}\,\text{kg}}{6.371 \times 10^6\,\text{m} + 600 \times 10^3\,\text{m}}} \tag{2.12}$$

$$= \sqrt{\frac{3.986 \times 10^{14}\,\text{m}^3\,\text{s}^{-2}}{6.971 \times 10^6\,\text{m}}} \tag{2.13}$$

$$= \sqrt{5.717 \times 10^7\,\text{m}^2\,\text{s}^{-2}} \approx 7556\,\text{m}\,\text{s}^{-1} \tag{2.14}$$

Radial Velocity and Elevation Angle

The satellite's motion contributes to the Doppler shift via its radial velocity component relative to the receiver [24]:

$$v_r = v_s \cdot \cos(\alpha) \tag{2.15}$$

where α represents the elevation angle between the satellite and the receiver, with $\alpha = 0°$ at the horizon and $\alpha = 90°$ directly overhead.

Substituting into the Doppler formula yields:

$$f_d = \frac{v_s \cdot \cos(\alpha)}{c} \cdot f_c \tag{2.16}$$

This formulation demonstrates that maximum Doppler shift occurs at low elevation angles near the horizon, decreases as the satellite moves overhead, and becomes zero at zenith ($\alpha = 90°$) where the radial velocity component vanishes.

To accurately account for satellite-ground link geometry, the radial velocity must be scaled by [24]:

$$\frac{R_e}{R_e + h} \tag{2.17}$$

This scaling factor compensates for the apparent reduction in satellite velocity from the receiver's perspective due to Earth's curvature and the satellite's altitude, effectively projecting the orbital velocity onto Earth's surface.

Thus, the adjusted radial component becomes:

$$v_r = v_s \cdot \frac{R_e}{R_e + h} \cdot \cos(\alpha) \tag{2.18}$$

Including Receiver Motion

In mobile user scenarios such as vehicular user equipment, the receiver's motion must also be incorporated:

$$f_d = \frac{1}{c}\left[v_s \cdot \frac{R_e}{R_e + h} \cdot \cos(\alpha) \pm v_{\text{rx}} \cdot \cos(\alpha)\right] \cdot f_c \tag{2.19}$$

where v_{rx} represents the receiver speed (for example, a vehicle traveling at $120\,\text{km}\,\text{h}^{-1}$ equates to $33\,\text{m}\,\text{s}^{-1}$), and the sign $\pm$ depends on whether the user equipment is moving toward (positive) or away from (negative) the satellite.

2.4 Link Budget Analysis

Accurately evaluating the quality and feasibility of wireless links in NTNs requires a comprehensive link budget analysis. The fundamental relationship between transmitted and received power in satellite communication systems can be expressed as:

$$P_r = P_t + G_t + G_r - L_{\text{FSPL}} - L_{\text{atm}} - L_{\text{other}} \tag{2.20}$$

In this comprehensive expression, P_r represents the received power in dBW, P_t denotes the transmitted power in dBW, G_t and G_r are the transmit and receive antenna gains in dBi respectively, L_{FSPL} accounts for free-space path loss in dB, L_{atm} encompasses atmospheric losses in dB, and L_{other} represents additional system losses in dB.

Figure 2.8 illustrates the complete signal chain from transmitter to receiver, showing how each component contributes to the overall link budget.

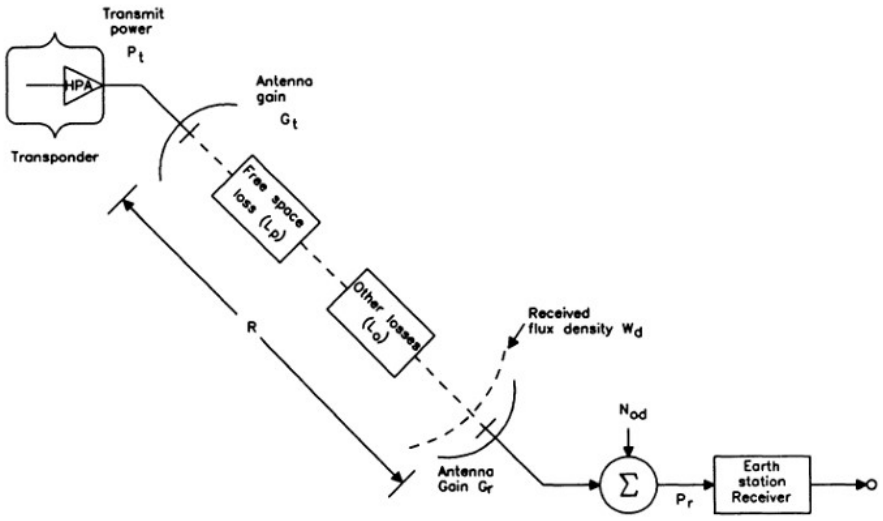

Figure 2.8: Satellite communication link budget components [35].

The transmit side is characterized by the Effective Isotropic Radiated Power (EIRP), calculated as $P_t + G_t$ in dBW. Antenna gains G_t and G_r quantify how much the antennas concentrate power in specific directions compared to ideal isotropic radiators, with higher gains significantly improving link performance.

The propagation path introduces several loss components. Free-space path loss L_{FSPL} follows the Friis transmission equation as defined in Equation 2.2, depending on carrier frequency and slant range. Atmospheric losses L_{atm} encompass gaseous absorption, rain attenuation, cloud effects, and scintillation, modeled using ITU-R recommendations P.676 and P.618. Additional losses L_{other} may include polarization mismatch, pointing errors, and implementation losses.

The noise power at the receiver is determined by the thermal noise equation $P_N = kT_S B_N$, where k is Boltzmann's constant, T_S is the system noise temperature, and B_N is the receiver bandwidth. The final link quality is quantified by the carrier-to-noise ratio, which directly impacts system performance metrics such as bit error rate and throughput. This comprehensive link budget formulation provides the foundation for evaluating NTN performance across various deployment scenarios and environmental conditions.

2.5 Performance Metrics Calculation

The evaluation of NTN system performance relies on five fundamental metrics that collectively quantify link quality, data integrity, and communication timing. These metrics provide a comprehensive framework for assessing the viability of satellite-based vehicular communications across various operational scenarios and environmental conditions.

2.5.1 Carrier-to-Noise Ratio

The CNR quantifies the ratio of received carrier power to noise power at the receiver. It is related to the carrier-to-noise density ratio (C/N_0) and the receiver bandwidth B as [23]:

$$\frac{C}{N}\ [\text{dB}] = \frac{C}{N_0}\ [\text{dB} - \text{Hz}] - 10\log_{10}(B\ [\text{Hz}]) \tag{2.21}$$

The (C/N_0) can be expressed in terms of system parameters as [23]:

$$\frac{C}{N_0}\ [\text{dB} - \text{Hz}] = \text{EIRP}\ [\text{dB}W] + \left(\frac{G}{T}\right)\ [\text{dB}/K] - L_s\ [\text{dB}] - k_{\text{dB}} \tag{2.22}$$

where EIRP represents the effective isotropic radiated power of the transmitter in dBW, G/T denotes the receiver antenna gain-to-noise-temperature ratio in dB/K, L_s accounts for the total space and atmospheric losses in dB, and $k_{\text{dB}} = -228.6$ dBW/K/Hz represents Boltzmann's constant in decibel form.

2.5.2 Energy per Bit to Noise Density Ratio

For digital communication systems, an important figure of merit is the ratio of the energy per bit to the noise power spectral density, denoted as E_b/N_0. This parameter provides a normalized measure of link quality that is independent of bandwidth and modulation format, making it particularly useful for evaluating BER performance [16].

$$\frac{E_b}{N_0}\ [\text{dB}] = \frac{C}{N_0}\ [\text{dB} - \text{Hz}] - 10\log_{10}\Big(R_b\ [\text{bit}\,\text{s}^{-1}]\Big) \tag{2.23}$$

where R_b is the information bit rate [bit s^{-1}].

In satellite communications, achieving a sufficient E_b/N_0 is crucial to ensure acceptable BER levels, especially under varying link conditions such as Doppler shift and atmospheric attenuation [5], [23].

2.5.3 Bit Error Rate (BER)

The bit error rate quantifies the probability of bit errors during transmission and serves as the ultimate measure of communication reliability. For additive white Gaussian noise channels with coherent detection, the BER for various modulation schemes follows well-established relationships [16]:

$$P_e = \begin{cases} Q\left(\sqrt{\frac{2E_b}{N_0}}\right) & \text{(BPSK)} \\ Q\left(\sqrt{\frac{E_b}{N_0}}\right) & \text{(QPSK)} \\ \frac{3}{2}Q\left(\sqrt{\frac{4}{5}\frac{E_b}{N_0}}\right) & \text{(16-QAM)} \\ \frac{7}{12}Q\left(\sqrt{\frac{2}{7}\frac{E_b}{N_0}}\right) & \text{(64-QAM)} \end{cases} \tag{2.24}$$

where $Q(\cdot)$ represents the Q-function. These relationships demonstrate the direct trade-off between spectral efficiency and error performance in NTN systems. The BER requirement varies significantly based on application, ranging from 10^{-3} for voice communications to 10^{-6} or lower for data transmission and mission-critical applications [5], [15].

2.5.4 Doppler Shift

Doppler shift is an important performance metric that measures how much the signal frequency changes due to satellite and vehicle movement. In LEO satellite systems, this effect is especially strong and can seriously impact communication quality [5], [24].

The frequency changes in satellite links are large enough that they require special correction methods. Without proper compensation, these frequency shifts can disrupt the careful timing between signals in OFDM systems, making it harder to decode information correctly [6]. The speed at which the frequency changes also affects how quickly the receiver needs to adapt, which adds complexity to the system design.

Tracking Doppler shift helps us understand when the communication link might be struggling. When frequency changes aren't properly handled, we see more errors in the received data and slower overall data speeds. This is particularly important for vehicle communications, where both the satellite and the vehicle are moving, creating complicated frequency patterns that the system must handle [7]. Managing these frequency changes properly is key to maintaining reliable connections in satellite-based vehicle communication systems.

2.5.5 Throughput Calculation

The effective throughput quantifies the net data rate successfully delivered over the link, accounting for transmission efficiency and bit errors. In this work, the effective throughput R_{eff} (in megabits per second, $\text{Mbit}\,\text{s}^{-1}$) is expressed as:

$$R_{\text{eff}} = \frac{N_{\text{bits}}}{T_{\text{total}}} \cdot (1 - P_e) \cdot 10^{-6} \tag{2.25}$$

where the total number of transmitted bits is given by $N_{\text{bits}} = N_{\text{sub}} \times N_{\text{sym}} \times \log_2(M)$, the total transmission time is $T_{\text{total}} = N_{\text{sym}} \times T_{\text{sym}}$, and the OFDM symbol duration is $T_{\text{sym}} = T_s + T_{\text{cp}}$. The useful symbol period is defined as $T_s = 1/\Delta f$, while the cyclic prefix duration is $T_{\text{cp}} = \frac{N_{\text{cp}}}{N_{\text{sub}}} \times T_s$. Additionally, P_e represents the bit error rate (BER) and M denotes the modulation order [16], [36].

This formulation reflects the fact that the raw transmission rate is reduced by error events, with the factor $(1 - P_e)$ representing the fraction of correctly received bits. The 10^{-6} scaling converts the result from bits per second to megabits per second ($\text{Mbit}\,\text{s}^{-1}$).

2.5.6 Latency Calculation

Latency is influenced by both propagation delays and the numerology used in 5G NR systems. Given the large slant distances between satellites and ground terminals, propagation delay becomes a dominant contributor, particularly at low elevation angles. Additionally, the choice of numerology (μ), which defines subcarrier spacing and slot duration significantly impacts transmission latency.

The total one-way physical layer latency is then modeled as the sum of the propagation and transmission components [32]:

$$t_{\text{total}} = t_p + t_t \tag{2.26}$$

This combined metric captures the fundamental delay experienced in NTN links, with t_p dominating at low elevation angles and t_t depending on the selected numerology.

2.5.6.1 Propagation Delay Analysis

The satellite-to-ground link introduces a non-negligible propagation delay due to the long slant range. The propagation delay t_p is calculated as [23]:

$$t_p = \frac{d}{c} \tag{2.27}$$

where d represents the slant range distance in meters and $c = 3 \times 10^8 \text{m}\,\text{s}^{-1}$ is the speed of light.

As shown in Figure 2.9, for a LEO satellite at an elevation angle of 90°, the slant range is approximately 600 km, corresponding to a 2 ms delay. At lower elevation

angles like 10°, the slant range increases to over 1000 km, resulting in a propagation delay of approximately 3.58 ms.

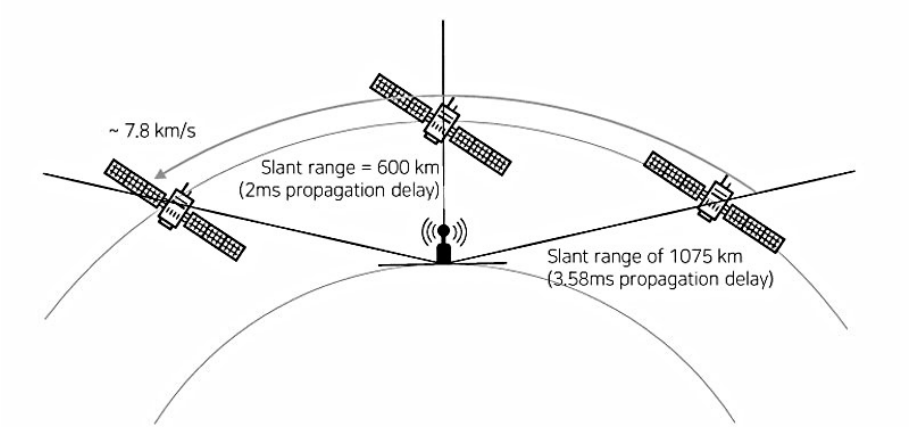

Figure 2.9: Propagation delay variation with elevation angle

2.5.6.2 Transmission Delay Based on Numerology

In 5G NR, the transmission delay is linked to the subcarrier spacing (Δf) determined by the numerology index μ [36]:

$$t_t = \frac{1}{2^\mu} \tag{2.28}$$

Each subframe has a fixed duration of 1 ms, but increasing μ results in shorter symbol and slot durations, allowing for more slots per subframe and potentially reduced latency. Figure 2.10 illustrates the 5G NR frame and slot structure for different numerologies [36].

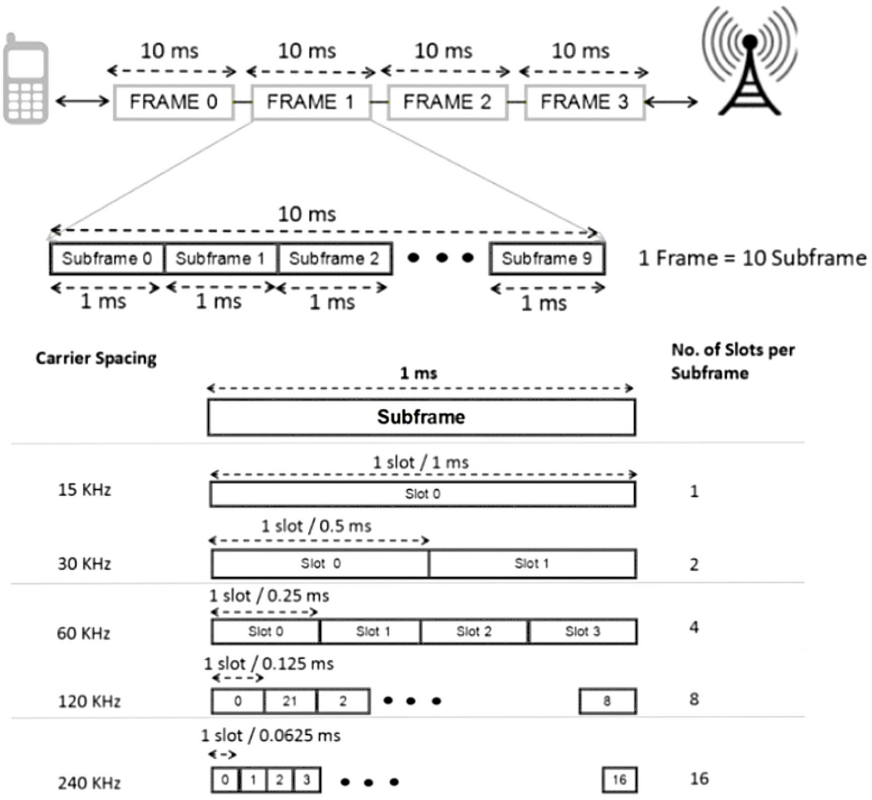

Figure 2.10: Frame and slot structure for different numerologies [37].

3

Methodology

This chapter details the methodology employed to evaluate the performance of satellite networks in supporting vehicular communications. The method combines theory with computer simulations to evaluate performance in different real-world situations.

The process follows five main steps that build on each other. First, the overall simulation plan and workflow are introduced to show how everything connects. Next, the computer tools and setup used for running the experiments are described. Then, the detailed implementation of the communication system is explained, showing how the signals are created and processed. After that, the various signal disruptions that happen in satellite links are modeled, including distance loss, weather effects, and frequency changes. Finally, the performance measures are defined to evaluate how well the system works, looking at signal quality, data speed, delays, and error rates.

This organized approach makes sure the testing process is logical and thorough, from setting up the simulation to measuring the final results.

3.1 Methodological Framework

This research uses a step-by-step approach that starts simple and gradually adds complexity to understand how each part of the system affects performance. Figure 3.1 shows the complete simulation process that forms the foundation of this study.

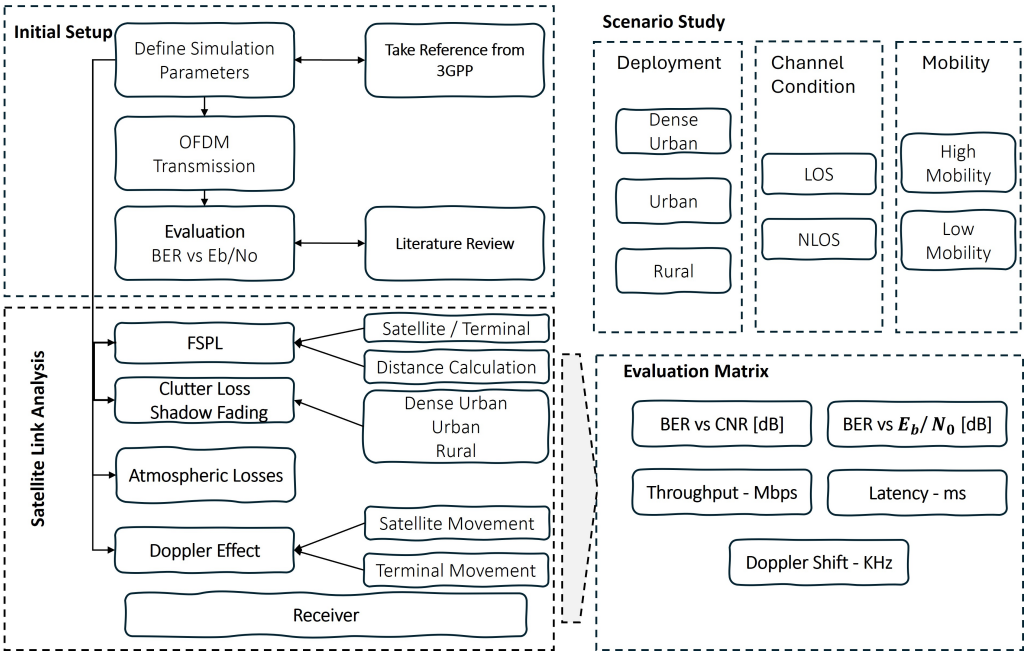

Figure 3.1: Simulation methodology for testing satellite network performance

The simulation process follows five main stages:

The first stage builds a basic communication system without any satellite-specific problems. This creates a simple OFDM wireless link using QPSK modulation and standard signal processing, providing a baseline system, helping to establish normal performance levels for later comparison.

The second stage gradually adds real-world satellite challenges one by one. It starts with signal loss due to distance, then adds weather effects, then frequency changes caused by movement, and finally environmental obstacles. Adding these effects separately helps to understand how much each one impacts the system.

The third stage calculates the complete power budget for the satellite link. This considers how much power is transmitted, how antennas focus the signal, how much signal is lost during transmission, and how much noise the receiver adds. The calculation follows standard formulas but includes special considerations for vehicles.

The fourth stage evaluates system performance using five key indicators. The carrier-to-noise ratio (CNR) is calculated to quantify signal quality. System reliability is characterized by measuring the Bit Error Rate (BER) through Monte Carlo simulations and plotting it against the energy-per-bit to noise ratio (E_b/N_0), which serves as a normalized measure of signal strength. Furthermore, throughput measures data speed, latency measures time delays, and Doppler shift measures frequency stability. All measurements are taken under controlled conditions to ensure accurate results.

The fifth stage tests the system in different real-world environments: rural areas with open spaces, urban areas with buildings, and dense cities with tall structures. Each

environment has different signal blocking characteristics, with rural areas having the least interference and dense cities having the most.

3.2 Implementation Environment

3.2.1 Simulation Platform and Configuration

All experiments were executed in MATLAB R2024b utilizing specialized toolboxes for comprehensive communications system analysis. The Communications Toolbox v8.6 provided fundamental signal processing functions including modulation, coding, and synchronization algorithms. The Satellite Communications Toolbox v5.5 enabled accurate modeling of satellite-specific propagation effects including atmospheric attenuation and orbital mechanics. The Signal Processing Toolbox supported advanced analysis and visualization capabilities for time-frequency analysis and statistical processing.

Simulation reproducibility was ensured through controlled random number generation with a fixed seed of 67890 across all experimental runs. Monte Carlo simulations employed $N = 100{,}000$ channel realizations to achieve statistical confidence in BER measurements down to 10^{-6} error rates, with the number of trials determined using binomial distribution confidence interval analysis. The computational framework strictly adheres to NTN channel and link models defined in 3GPP TR 38.811 V15.4.0 [5], with atmospheric propagation effects modeled according to ITU-R P.618-14 [20] and gaseous absorption following ITU-R P.676-12 [22]. Source code and detailed parameter settings are summarized in Appendix B to facilitate reproducibility.

3.2.2 Parameter Configuration and System Setup

The simulation framework implements two primary frequency bands selected based on 3GPP NTN study specifications and practical satellite system deployments. S-band operation at 2 GHz provides reference performance for current satellite services, while Ka-band at 20 GHz represents emerging high-throughput systems. The complete parameter configuration spans physical layer settings, satellite orbital parameters, and environmental conditions, with elevation angles varying from 10° to 90° to capture the full range of operational geometries.

Table 3.1: Simulation parameters for performance evaluation

Parameter	S-band	Ka-band
Carrier Frequency	2 GHz	20 GHz
Bandwidth	2 MHz	10 MHz
Satellite EIRP	43 dBW	65 dBW
UE Antenna Gain	12 dBi	25 dBi
Noise Figure	2 dB	1.5 dB
Satellite Altitude	600 km	600 km
Modulation	QPSK	QPSK
UE Speed	120 km/h	120 km/h
Environment	Rural	Rural
Monte Carlo Trials	100,000	10,000

3.3 OFDM System Implementation

3.3.1 Transmitter Chain Implementation

The OFDM transmitter implementation provides a functional simulation of satellite communication signals using standard digital signal processing techniques. The implementation focuses on core OFDM principles while making several simplifications for computational efficiency.

Binary data is converted to complex symbols using QPSK modulation, where each symbol carries two bits of information. The data symbols are distributed across 512 subcarriers using straightforward allocation without dedicated pilot subcarriers or guard band configurations. Time-domain signals are generated using inverse Fourier transform processing with cyclic prefix insertion. The cyclic prefix length is set to 64 samples, providing protection against delay spread while maintaining good spectral efficiency. A power normalization step is applied to maintain consistent signal levels across different transmission conditions.

3.3.2 Receiver Chain Implementation

The receiver processing mirrors the transmitter operations using corresponding demodulation techniques. The implementation assumes perfect synchronization, bypassing the need for timing and frequency offset recovery algorithms that would be essential in practical systems. Signal demodulation performs cyclic prefix removal and applies Fourier transform processing to recover frequency-domain symbols. QPSK demodulation then converts the symbols back to binary data.

3.4 Channel Impairment Modeling

3.4.1 Free-Space Path Loss Implementation

Free-space path loss calculations follow the 3GPP TR 38.811 model using geometric relationships for satellite links. The implementation computes the slant range between the satellite at 600 km altitude and ground terminal using elevation-angle-dependent geometry. Path loss is then calculated using the standard Friis transmission equation that accounts for both distance and carrier frequency effects.

The slant range calculation considers the spherical Earth geometry with a radius of 6,371 km, producing path distances that vary from approximately 1,900 km at 10° elevation to 600 km at 90° elevation. This geometric approach ensures accurate representation of the varying signal path lengths encountered in practical satellite operations.

3.4.2 Atmospheric Loss Modeling

Atmospheric losses are modeled using ITU-R P.618 recommendations adapted for non-terrestrial networks. The implementation calculates composite atmospheric attenuation values that depend on both carrier frequency and elevation angle. For S-band operations at 2 GHz, atmospheric losses remain relatively low, typically under 0.5 dB, while Ka-band at 20 GHz experiences more significant attenuation, particularly at lower elevation angles where the signal travels longer paths through the atmosphere.

The model incorporates frequency-dependent effects including gaseous absorption and rain attenuation, with elevation angle scaling applied to account for the varying atmospheric path lengths. This simplified approach provides realistic attenuation estimates while maintaining computational efficiency for the Monte Carlo simulations.

3.4.3 Doppler Shift Calculation

Doppler shift is computed based on the relative motion between the LEO satellite orbiting at 7.5 km/s and the ground vehicle moving at 120 km/h. The implementation calculates the radial velocity component using satellite orbital geometry and elevation angle relationships, then applies the standard Doppler formula to determine the frequency shift.

For the 600 km altitude satellite, Doppler shifts range from several kilohertz at zenith to over 50 kHz at low elevation angles, with Ka-band experiencing proportionally larger shifts due to the higher carrier frequency. The simulation models both satellite-to-vehicle approaching and receding scenarios, though it applies the Doppler shift as a bulk frequency offset rather than implementing dynamic tracking algorithms.

3.4.4 Environmental Fading Effects

Environmental effects are modeled using large-scale fading parameters from 3GPP TR 38.811, with different loss characteristics applied for rural, urban, and dense urban scenarios. The implementation combines fixed clutter loss values with log-normal shadow fading to represent the variability in signal strength due to terrain and obstacles.

Table 3.2: Channel parameters per scenario (based on 3GPP TR 38.811)

Scenario	**Shadowing Mean** (dB)	**Shadowing σ** (dB)		**Clutter Loss** (dB)		**Notes**
		S-band	**Ka-band**	**S-band**	**Ka-band**	
Rural	0	2–4	2–3	25–34	33–44	Clear-sky, open terrain
Suburban	0	3–4	2–3	29–39	37–48	Mixed foliage/buildings
Urban	0	2–3	2–3	33–42	41–52	Street canyons
Dense Urban	0	2–3	2–3	36–43	45–53	High-rise cores

Rural environments exhibit the lowest additional losses with minimal shadowing variation, while dense urban scenarios introduce the most challenging propagation conditions with significant clutter loss and building shadowing effects. The parameter ranges account for the different frequency-dependent behaviors observed at S-band and Ka-band.

3.5 Performance Evaluation Framework

System performance is evaluated using five key metrics that collectively characterize link quality and communication reliability. Each metric is computed directly from the simulation outputs using standardized relationships.

The carrier-to-noise ratio (CNR) is calculated from the complete link budget, considering transmitted power, antenna gains, all propagation losses, and receiver noise characteristics. The bit error rate (BER) is measured by comparing transmitted and received data bits across multiple trials. Since the BER is inherently dependent on the instantaneous link quality, its performance is characterized as a function of both the CNR and the derived E_b/N_0. These fundamental relationships BER versus CNR and BER versus E_b/N_0 enable a comprehensive analysis of the link's reliability from both a high-level link-budget perspective and a fundamental modulation-and-coding perspective. Finally, the throughput is computed as the effective data rate successfully delivered to the receiver, accounting for both physical layer efficiency and performance degradation due to bit errors.

Latency is computed as the sum of propagation delay and transmission delay components. Propagation delay depends on the geometric slant range between satellite and ground terminal, while transmission delay is determined by 5G NR numerology settings. The combined calculation provides realistic timing estimates for satellite link performance assessment across different elevation angles and system configurations.Doppler shift is monitored as an indicator of frequency stability and synchronization requirements, though the current implementation does not include dynamic compensation mechanisms.

4

Results

This chapter presents the performance evaluation of LEO satellite communication systems for vehicular applications, following the methodological framework established in Figure 3.1 and using the simulation parameters defined in Table 3.1. The analysis systematically examines the key performance metrics—BER versus CNR, BER versus E_b/N_0, throughput, latency, and Doppler shift—across different operational scenarios. The evaluation considers both S-band and Ka-band frequencies operating with a 600 km LEO satellite, with performance assessed across elevation angles from 10° to 90° to capture the full range of geometric conditions. The results are organized to follow the logical progression of the evaluation methodology, beginning with fundamental link reliability analysis through BER performance, progressing to data delivery performance through throughput evaluation and timing characteristics via latency assessment, concluding with frequency stability analysis through Doppler shift examination.

4.1 BER versus E_b/N_0 Analysis

This section analyzes the bit error rate as a function of E_b/N_0 to evaluate fundamental link reliability under varying channel conditions. The results demonstrate the critical relationship between elevation angle and communication performance, considering both S-band and Ka-band operation in rural environments with shadow fading and clutter loss representing realistic deployment scenarios.

Table 4.1 presents the performance of BER and E_b/N_0 across elevation angles from 10° to 90°. The results reveal a clear progression in performance from unusable conditions at low elevations to near error-free operation at high elevations. At 10° elevation, both frequency bands experience severe degradation with negative E_b/N_0 values and BER exceeding 0.35, indicating the necessity for advanced error correction in challenging geometric conditions. Performance improves substantially at intermediate elevations, with both bands achieving positive E_b/N_0 above 30° and BER decreasing to approximately 10^{-3} at 50° elevation, representing marginal but usable link quality. Excellent performance is achieved at high elevations, with both bands reaching near error-free operation (BER $< 10^{-6}$) at 90° elevation.

Table 4.1: BER and E_b/N_0 performance across elevation angles

Elevation Angle (°)	**S-band**		**Ka-band**	
	BER	$\boldsymbol{E_b/N_0}$ **[dB]**	**BER**	$\boldsymbol{E_b/N_0}$ **[dB]**
10	0.353	-13.26	0.44	-15.38
30	8.35e-2	-0.41	0.141	3.24
50	6.66e-3	4.99	9.43e-3	11.01
70	1.74e-4	8.21	4.36e-4	14.08
90	2.80e-6	10.31	1.43e-6	17.07

The BER versus E_b/N_0 relationships provide visual confirmation of the performance trends identified in the table. Figure 4.1 illustrates the S-band characteristics, demonstrating reliable operation above 50° elevation with progressive improvement as elevation increases. Figure 4.2 shows the Ka-band performance, revealing similar reliability patterns despite requiring higher E_b/N_0 values across all elevation angles. The consistent improvement across elevation angles for both frequency bands confirms the fundamental importance of geometric link conditions for satellite communication reliability.

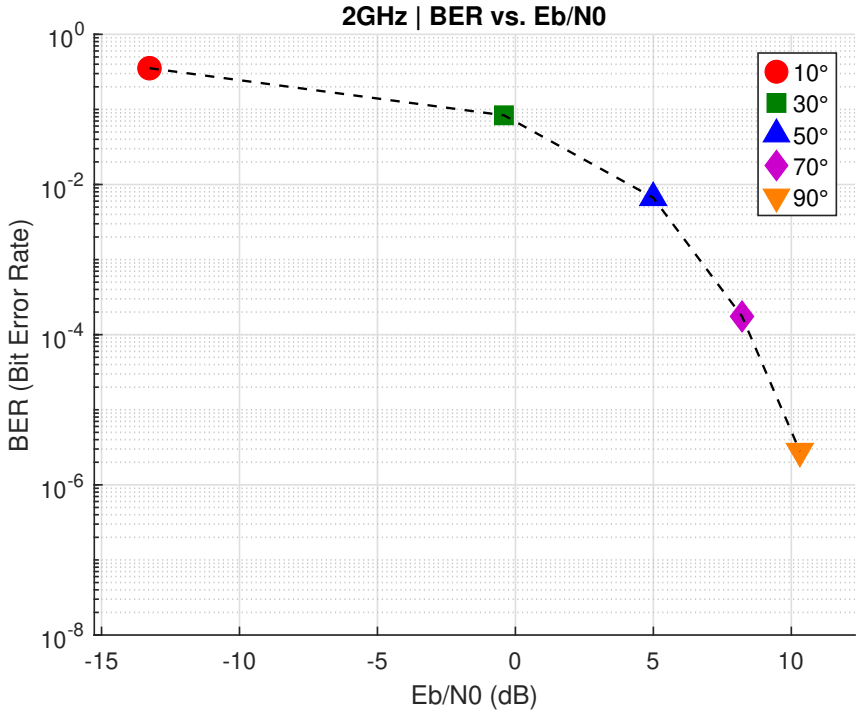

Figure 4.1: S-band BER vs. E_b/N_0 for different elevation angles.

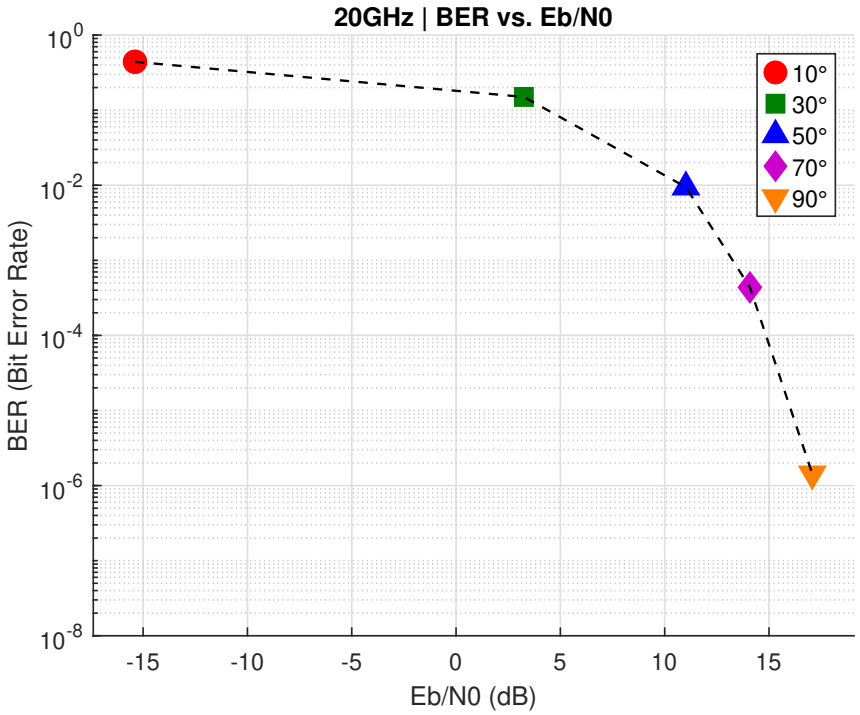

Figure 4.2: Ka-band BER vs. E_b/N_0 for different elevation angles.

The performance comparison reveals that Ka-band requires approximately 6-7 dB higher E_b/N_0 than S-band for equivalent BER performance, attributable to higher implementation losses and more severe phase noise effects at millimeter-wave frequencies. Despite this requirement, Ka-band achieves superior E_b/N_0 performance at high elevations (17.07 dB versus 10.31 dB at 90°), suggesting better potential for high-throughput applications under favorable link conditions. This trade-off between frequency band selection and performance requirements highlights the importance of matching system design to specific operational scenarios and elevation angle constraints.

4.2 BER versus CNR Analysis

The BER versus CNR analysis provides a comprehensive assessment of overall link quality by incorporating all major channel impairments including path loss, atmospheric attenuation, shadow fading, and clutter loss. This metric offers a complete view of link performance under rural deployment conditions, complementing the E_b/N_0 analysis with a system-level perspective.

Table 4.2 presents the BER and CNR performance across elevation angles, revealing consistent patterns despite different frequency characteristics. The results show that both S-band and Ka-band require approximately 15 dB CNR to achieve reliable communication with BER below 10^{-6}, establishing a universal performance threshold. The CNR improvement with elevation angle demonstrates significant enhancement, with approximately 30 dB improvement from 10° to 90° elevation across both frequency bands.

Table 4.2: BER and CNR performance across elevation angles

Elevation Angle (°)	**S-band**		**Ka-band**	
	BER	**CNR [dB]**	**BER**	**CNR [dB]**
10	0.353	-6.51	0.44	-15.01
30	8.35e-2	4.81	0.141	1.82
50	6.66e-3	9.87	9.43e-3	8.92
70	1.74e-4	13.07	4.36e-4	11.95
90	2.80e-6	15.16	1.43e-6	14.94

The BER versus CNR relationships provide visual confirmation of the consistent performance thresholds identified in the table. Figure 4.3 illustrates the S-band characteristics, demonstrating the clear progression toward reliable operation as CNR approaches 15 dB. Figure 4.4 shows the Ka-band performance, revealing nearly identical CNR requirements despite the frequency band differences. The consistent behavior across both frequency bands confirms CNR as a universal link quality metric for system design.

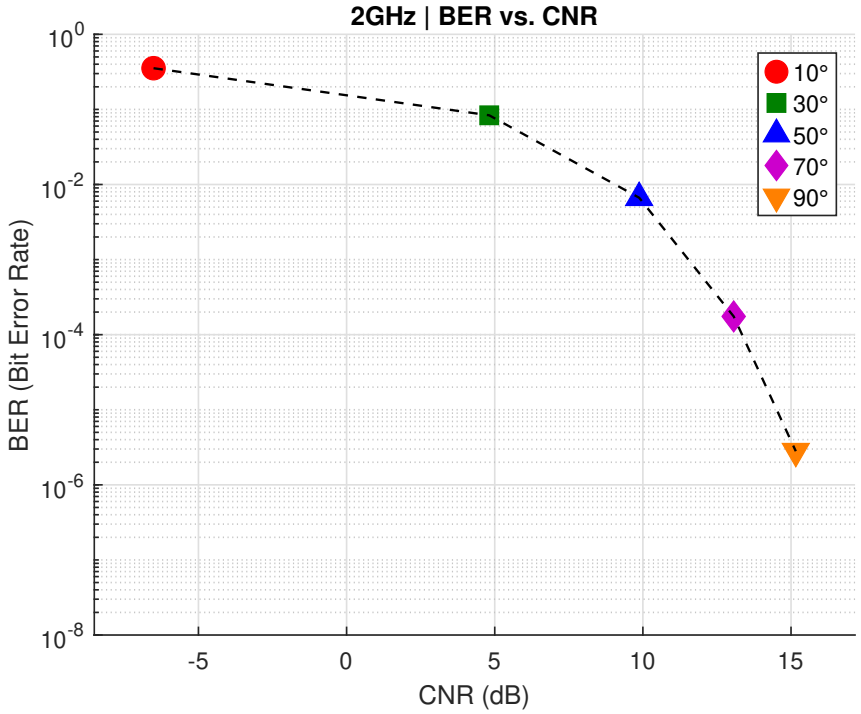

Figure 4.3: S-band BER vs.CNR for different elevation angles.

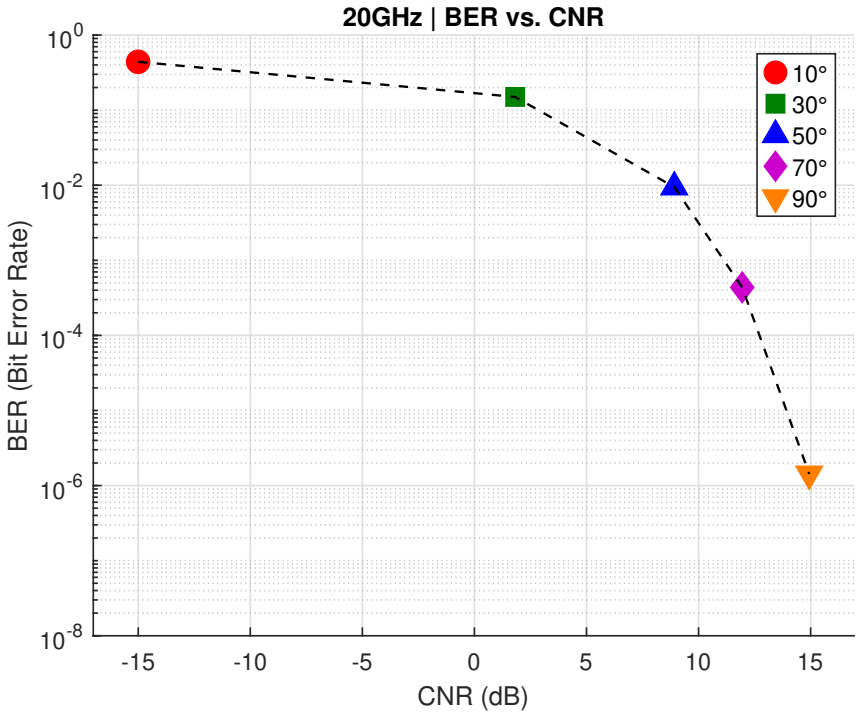

Figure 4.4: Ka-band BER vs.CNR for different elevation angles.

The analysis reveals that despite Ka-band's higher E_b/N_0 requirements identified in the previous section, both frequency bands exhibit nearly identical CNR requirements for equivalent BER performance. This consistency suggests that the additional implementation losses at Ka-band are effectively captured within the CNR metric, providing system designers with a universal target of 15 dB CNR for reliable operation. The establishment of this common threshold enables simplified system design regardless of frequency selection, though practical implementation considerations may still favor S-band for better low-elevation performance or Ka-band for higher capacity potential at favorable elevations.

4.3 Throughput Performance

The throughput analysis evaluates the effective data delivery capacity of satellite links, calculated using the formulation established in Section 2.5.5 that accounts for total transmitted bits, symbol duration, and bit error rate effects. This metric provides crucial insights into practical system performance beyond basic link quality measures.

Figure 4.5 illustrates the throughput performance across elevation angles from 10° to 90°, revealing clear performance advantages for Ka-band operation. The results demonstrate consistent throughput improvement with increasing elevation angle for both frequency bands, driven by enhanced link quality and reduced bit error rates at higher elevations. Ka-band achieves significantly higher throughput across all elevation angles, with performance approximately 4-5 times greater than S-band due

to the larger allocated bandwidth supporting higher symbol rates and increased data capacity.

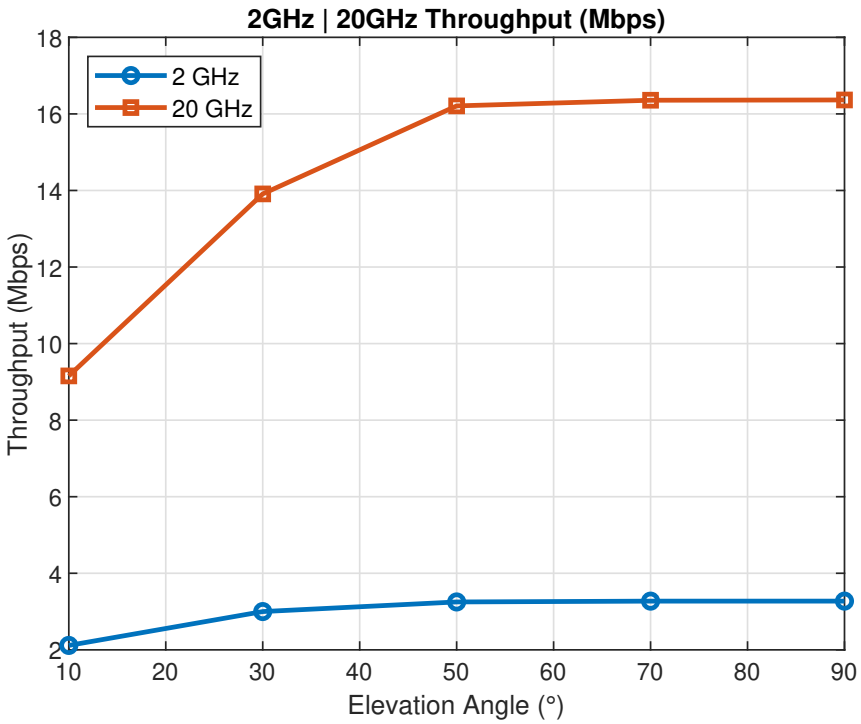

Figure 4.5: Throughput performance analysis.

The performance comparison reveals maximum throughput rates approaching 8 Mbps for Ka-band at 90° elevation, compared to approximately 1.5 Mbps for S-band under the same conditions. This substantial difference highlights Ka-band's superiority for high-capacity applications, though both bands maintain usable throughput above 30° elevation. The elevation-dependent performance improvement follows expected patterns, with throughput enhancement directly correlated with improved link quality metrics identified in previous sections. The results confirm that while S-band provides adequate performance for basic communication needs, Ka-band offers significant advantages for applications requiring higher data rates, provided that favorable elevation angles can be maintained.

4.4 Latency

In this simulation, latency refers to the one-way physical layer latency, which includes the propagation delay and the transmission delay as defined in Section 2.5.6. Processing delays at the transceiver and higher-layer protocol overheads are excluded, since the focus of this study is strictly on physical layer performance.

The simulation results in Figure 4.6 demonstrate how latency decreases with higher elevation angles and larger numerology indices. Specifically:

- For $\mu = 0$ (15 kHz), latency is highest across all elevation angles.

- As μ increases to 1, 2, 3, and 4, the slot duration becomes shorter, resulting in reduced latency.
- At elevation angles close to 90°, the impact of propagation delay diminishes, and numerology becomes the key latency-reduction factor.
- Conversely, at lower elevation angles, the propagation delay dominates, limiting the overall latency gains achievable from higher numerologies.

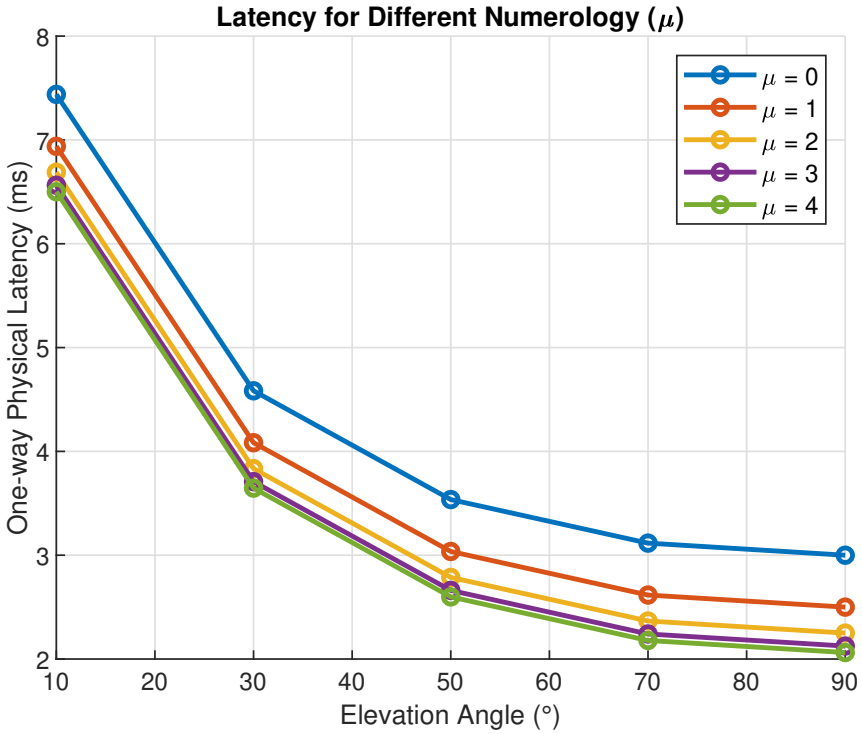

Figure 4.6: Latency vs elevation angle for different numerologies

From a practical standpoint, these findings highlight the need to optimize both link geometry and numerology configuration to meet the latency requirements, especially in use cases like autonomous vehicles and remote control systems, where the target end-to-end latency is often below 5 ms [5].

4.5 Doppler Shift: Impact of Mobility Direction

The Doppler shift analysis provides insight into the frequency stability challenges encountered in LEO-based communication systems. As expected, the magnitude of the Doppler offset increases linearly with the carrier frequency. Under stationary user conditions, the S-band exhibits a Doppler shift of approximately 46 kHz, whereas the Ka-band reaches nearly 460 kHz. This tenfold increase is consistent with the frequency ratio and indicates that higher-frequency NTN links require substantially more sophisticated synchronization mechanisms.

User mobility introduces only minor deviations from the stationary case, with

variations of roughly ±0.5% across all mobility directions. While this percentage change is small, the corresponding absolute offsets—particularly the 463 kHz shift observed at Ka-band—pose significant challenges for OFDM systems, as even small frequency errors can lead to inter-carrier interference. These results highlight the importance of accurate Doppler estimation and compensation for high-frequency NTN deployments, especially in vehicular environments where relative motion is inevitable.

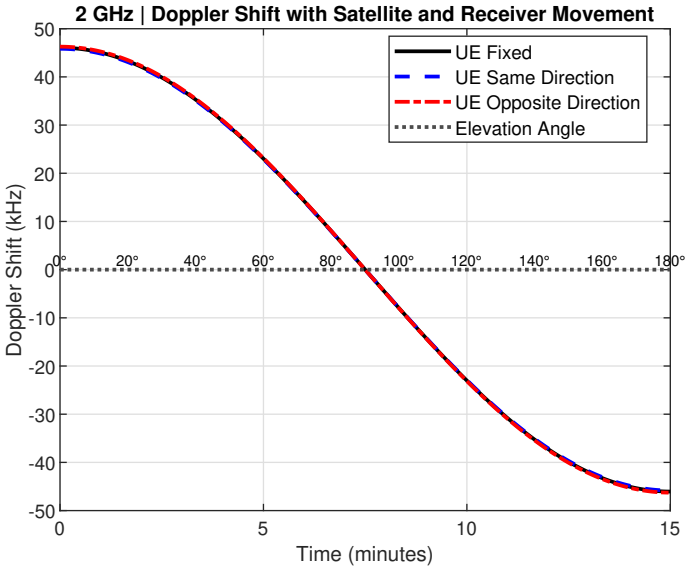

Figure 4.7: Doppler shift at 2 GHz for fixed, same-direction, and opposite-direction mobility scenarios.

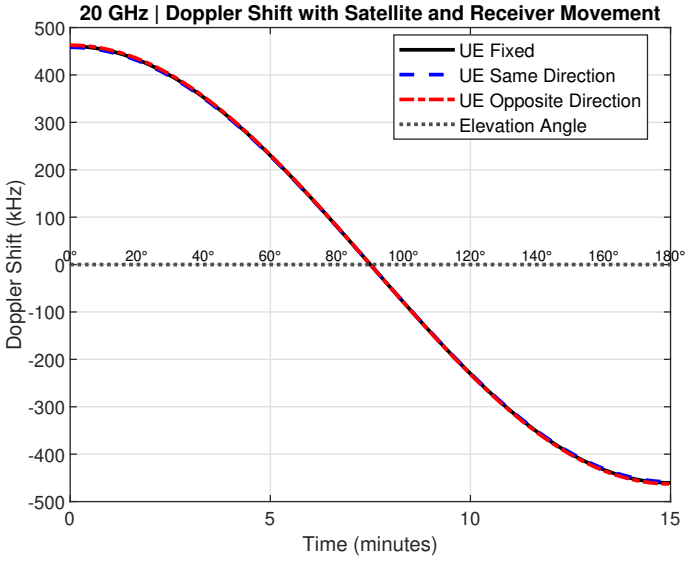

Figure 4.8: Doppler shift at 20 GHz.

Table 4.3 summarizes the Doppler values for both bands and all mobility cases. The results confirm that while mobility has a limited relative impact, the absolute

Doppler shift—particularly at Ka-band—remains a dominant factor affecting link stability.

Table 4.3: Doppler shift values at S-band and Ka-band under different mobility directions

Frequency (GHz)	**Fixed** (kHz)	**Same Dir.** (kHz)	**Opp. Dir.** (kHz)	**Δ Same**	**Δ Opp.**
2	46.05	45.82	46.27	-0.23	+0.22
20	460.52	458.29	462.74	-2.23	+2.22
Relative deviation: ±0.48%					

Overall, the results show that Doppler shift is primarily dominated by carrier frequency rather than user mobility. Nevertheless, given the large absolute Doppler values at higher bands, especially the Ka-band, precise frequency tracking and compensation strategies remain essential for maintaining reliable OFDM-based NTN communication.

4.6 Key Findings

The analysis has revealed several important patterns that shape the performance of NTN links. These patterns highlight how system design choices and operating conditions directly influence link reliability and efficiency. The most notable findings are summarised below.

- **Elevation angle critically determines link quality.** Higher elevation angles reduce slant range and path loss, leading to improvements across all key metrics: CNR, E_b/N_0, BER, throughput, and latency. For instance, CNR increases by more than 25 dB between 10° and 90° elevation (Tables 4.2), resulting in BER reductions from > 0.3 at 10° to $< 10^{-6}$ at 90°.
- **Environmental losses dominate at low elevations.** Shadow fading (SF) and clutter loss (CL) impose an additional 27 dB–47 dB penalty compared to free-space path loss, with Ka-band consistently suffering ∼8 dB–10 dB more degradation than S-band due to its higher susceptibility to propagation impairments [5], [20]. This additional margin must be included in link budgets for rural and urban NTN deployments.
- **Bandwidth constraints at lower frequencies.** S-band is robust against environmental losses but offers limited throughput due to narrow regulatory allocations (often 10 MHz) and legacy MSS use [5], [38]. In contrast, Ka-band can exploit wider bandwidths, achieving higher throughput under identical conditions (Figure 4.5). However, this comes at the cost of higher sensitivity to fading and atmospheric attenuation.
- **BER thresholds guide system design.** Simulations confirm that maintaining $E_b/N_0 > 10$dB or CNR > 15 dB ensures BER $< 10^{-4}$ aligning with reliability requirements for mission-critical NTN applications. These values can serve as practical design goals.

- **Latency depends jointly on geometry and numerology.** At 90° elevation, propagation delay is minimized (∼2.25 ms for LEO at 600 km altitude). Using higher numerologies (e.g., $\mu = 4$) reduces slot duration to 62.5 µs, cutting transmission delay further and supporting URLLC use cases such as autonomous vehicle control (Figure 4.6) [39]. At low elevations, however, propagation delay dominates and limits gains achievable from numerology scaling.
- **Doppler shift scales linearly with carrier frequency but proportionally remains small.** For LEO at 600 km and orbital velocity ∼7.6 km s^{-1}, Doppler reaches ∼46 kHz at 2 GHz and ∼462 kHz at 20 GHz. Relative to carrier frequency, this is ∼0.0023% in both cases. Nonetheless, uncompensated Doppler can degrade OFDM orthogonality and must be mitigated via synchronization techniques [23], [32].
- **Urban and dense-urban environments amplify path loss.** CL and SF increase losses as compared to baseline free-space conditions. For example, dense urban NTN adds ∼35 dB excess loss at 2 GHz and over 40 dB at 20 GHz (Appendix A.5), demanding adaptive power control, coding, or hybrid terrestrial-satellite integration to sustain QoS [32], [40].

These insights offer a practical framework for optimizing NTN system design by carefully balancing four critical aspects:

- **Throughput:** Trade-off between spectrum availability and frequency band selection.
- **Latency:** Jointly optimized via elevation geometry and numerology.
- **Reliability:** Ensured when E_b/N_0 and CNR exceed practical thresholds (∼10 dB and 15 dB respectively).
- **Robustness:** Maintained through mitigation of environmental impairments using adaptive antennas, diversity, coding, and power control.

5

Conclusion

5.1 Discussion

This study evaluated the performance of LEO satellite-based NTN links using a simulation framework that incorporated free-space path loss, Doppler shift, atmospheric attenuation, and environmental losses. The results confirm that elevation angle is the dominant factor influencing link quality: higher angles reduce slant range and Doppler, improving CNR, BER, throughput, and latency.

Ka-band enables higher throughput due to wider bandwidths (Figure 4.5), but is more vulnerable to atmospheric and environmental losses [20]. By contrast, S-band offers greater robustness, though with limited capacity due to narrower spectrum allocations [5], [38]. Environmental impairments such as shadow fading and clutter loss add 27 dB–47 dB of excess loss, often rendering low-elevation links unusable. Reliable performance (BER $< 10^{-6}$) requires CNR $\geq$15 dB, achievable at higher elevations or with additional EIRP and antenna gains.

These findings highlight the key trade-offs in NTN design: S-band for reliability and coverage, Ka-band for capacity; elevation planning as a critical parameter; and the need for adaptive techniques such as power control, beamforming, and diversity to maintain service quality under realistic conditions.

5.2 Conclusion

This thesis developed a simulation framework to assess LEO-based NTN links, quantifying the effects of elevation geometry, frequency choice, and environmental losses. The main conclusions are:

- **Elevation Dominates Feasibility:** Increasing elevation from 10° to 90° improves CNR by $\sim$22 dB at S-band and $\sim$30 dB at Ka-band (Table 4.2), establishing elevation as the primary determinant of link availability.
- **S-band Robustness vs. Ka-band Capacity:** S-band offers better resilience to shadow fading, clutter, and atmospheric losses, while Ka-band provides higher throughput (Table A.2) but requires stricter link budgets.
- **Severe SF/CL Penalties:** Shadow fading and clutter loss add 25 dB–30 dB of excess path loss in rural NTN environments, often rendering low-elevation

links unusable.

- **Performance Thresholds Defined:** Reliable operation (BER $< 10^{-6}$) requires CNR $\geq$15 dB across both bands (Table 4.2), providing a clear design target for link budgeting.
- **Recovery Requires Additional Margin:** Compensation of SF/CL penalties demands higher satellite EIRP, high-gain user antennas or strong coding schemes to close the performance gap.

These results confirm the feasibility of NTN integration into 5G/6G networks but show that success relies on careful elevation planning, band selection, and robust link design.

5.3 Future Work

Several research directions can extend this study toward more realistic and system-level insights:

- **Doppler Compensation:** Evaluate Automatic Frequency Control (AFC) and pilot-aided ICI cancellation to mitigate frequency offsets in high-mobility NTN links.
- **Advanced Coding and HARQ:** Quantify the impact of LDPC codes and HARQ on required CNR and achievable throughput under realistic error patterns.
- **Handover and Constellation Dynamics:** Model pass-to-pass and beam-to-beam handovers, including signaling overheads and failure rates, in large LEO constellations.
- **System-Level Design:** Extend analysis to constellation planning (LEO vs. MEO vs. GEO) and required satellite counts for continuous coverage.
- **Hardware Validation:** Integrate SDR-based experiments or NTN testbeds to validate simulation results under real Doppler and phase-noise conditions, particularly at Ka-band.

These directions will bridge the gap between link-level simulations and operational NTN deployment, supporting ongoing standardisation efforts.

Bibliography

[1] S. Liu, L. Liu, J. Tang, B. Yu, Y. Wang, and W. Shi, "Edge computing for autonomous driving: Opportunities and challenges," *Proc. IEEE*, vol. 107, no. 8, pp. 1697–1716, Aug. 2019. DOI: 10.1109/JPROC.2019.2915983.

[2] I. Leyva-Mayorga, B. Soret, M. Röper, *et al.*, "Leo small-satellite constellations for 5g and beyond-5g communications," *IEEE Access*, vol. 8, pp. 184 955–184 964, 2020. DOI: 10.1109/ACCESS.2020.3029620.

[3] O. Kodheli, E. Lagunas, N. Maturo, *et al.*, "Satellite communications in the new space era: A survey and future challenges," *IEEE Communications Surveys & Tutorials*, vol. 23, no. 1, pp. 70–109, 2021.

[4] M. Giordani and M. Zorzi, "Non-terrestrial networks in the 6g era: Challenges and opportunities," *IEEE Network*, vol. 34, no. 5, pp. 244–251, 2020.

[5] 3GPP, "Study on new radio (nr) to support non-terrestrial networks (release 15)," 3rd Generation Partnership Project, Technical Report TR 38.811, version 15.1.0, 2019. [Online]. Available: https://www.3gpp.org.

[6] C. Corral *et al.*, "Doppler compensation in leo satellite communications," in *IEEE International Conference on Communications (ICC)*, 2020, pp. 1–6.

[7] F. Rinaldi *et al.*, "Waveform design for leo satellite systems," *IEEE Transactions on Vehicular Technology*, vol. 69, no. 6, pp. 6789–6801, 2020.

[8] Y. Li *et al.*, "Rain attenuation at ka-band for leo satellite communications," *IEEE Antennas and Wireless Propagation Letters*, vol. 18, no. 4, pp. 704–708, 2019.

[9] A. Guidotti and A. Vanelli-Coralli, "Link budget analysis for leo constellations," *IEEE Transactions on Aerospace and Electronic Systems*, vol. 56, no. 3, pp. 2426–2440, 2020.

[10] G. Araniti *et al.*, "Satellite-based vehicular communications," *IEEE Wireless Communications*, vol. 21, no. 5, pp. 62–71, 2014.

[11] J. Garcia-Sanchez *et al.*, "Hybrid satellite-terrestrial v2x architectures," in *IEEE Vehicular Networking Conference (VNC)*, 2020, pp. 1–4.

[12] A. Al-Hourani *et al.*, "Satellite communications for connected vehicles," *IEEE Transactions on Vehicular Technology*, vol. 68, no. 4, pp. 3153–3169, 2019.

[13] A. Shkurti *et al.*, "Communication requirements for autonomous driving systems," *IEEE Transactions on Intelligent Vehicles*, vol. 6, no. 2, pp. 234–248, 2021.

[14] T. Abbas *et al.*, "Vehicular communication: Standardization and open issues," *IEEE Communications Standards Magazine*, vol. 2, no. 4, pp. 74–80, 2018.

[15] 5. A. Association, "V2x functional and performance requirements," 5GAA, Technical Report, 2020.

[16] A. Goldsmith, *Wireless Communications*. Cambridge, U.K.: Cambridge University Press, 2005.

[17] J. Geier, *Designing and Deploying 802.11 Wireless Networks: A Practical Guide to Implementing 802.11n and 802.11ac Wireless Networks for Enterprise-Based Applications*, 5th. Pearson Education, 2015.

[18] C. E. Shannon, "A mathematical theory of communication," *The Bell System Technical Journal*, vol. 27, no. 3, pp. 379–423, 1948.

[19] D. Roddy, *Satellite Communications*, 4th. New York, NY, USA: McGraw-Hill, 2006.

[20] ITU-R, "Propagation data and prediction methods required for the design of earth-space telecommunication systems," International Telecommunication Union, Geneva, Switzerland, Recommendation P.618-14, 2019.

[21] C. Jeffrey, R. Munro, and R. Thirsk, *An Introduction to GNSS: A Primer in Using Global Navigation Satellite Systems for Positioning and Autonomy*. Hexagon, 2023.

[22] I. T. U. (ITU), "Attenuation by atmospheric gases and related effects," International Telecommunication Union, ITU-R Recommendation P.676-12, 2019.

[23] G. Maral and M. Bousquet, *Satellite Communications Systems: Systems, Techniques and Technology*, 5th. Chichester, U.K.: Wiley, 2009.

[24] M. Höyhtyä and A. Vanelli-Coralli, *Satellite Communications and Networks* (Textbooks in Telecommunication Engineering). Cham, Switzerland: Springer, 2024. DOI: 10.1007/978-3-031-72926-3.

[25] A. Görçin and H. Arslan, "An OFDM signal identification method for wireless communications systems," *IEEE Trans. Veh. Technol.*, vol. 64, no. 12, pp. 5688–5700, Dec. 2015. DOI: 10.1109/TVT.2015.2388671.

[26] S. Namdeo, "Designing and performance evaluation of 64-QAM OFDM system," *IOSR J. Electron. Commun. Eng.*, vol. 5, no. 6, pp. 97–105, 2013.

[27] D. K. Sharma, S. L. Peng, R. Sharma, and G. Jeon, *Micro-Electronics and Telecommunication Engineering: Proceedings of the 6th ICMETE 2022*. Springer Nature Singapore, 2023.

[28] J. G. Proakis and M. Salehi, *Digital Communications*, 5th. New York, NY, USA: McGraw-Hill, 2008.

[29] S. Yoon, M. Kang, and J.-Y. Choi, "Security attacks against the availability of low earth orbit satellite networks," in *Proceedings of the 12th International Conference on Networks, Communication and Computing (ICNCC '23)*, New York, NY, USA: Association for Computing Machinery, 2024, pp. 64–69. DOI: 10.1145/3638837.3638847.

[30] ITU-R, "Propagation data required for the design of earth-space land mobile telecommunication systems," International Telecommunication Union, Tech. Rep. P.681-11, 2019.

[31] ITU-R, "Prediction of clutter loss," International Telecommunication Union, Tech. Rep. P.2108-1, 2020.

[32] 3GPP, "Study on channel model for frequencies from 0.5 to 100 ghz (release 16)," 3rd Generation Partnership Project, Technical Report TR 38.901, version 16.1.0, 2020. [Online]. Available: https://www.3gpp.org.

[33] ITU-R, "Propagation data and prediction methods for the planning of short-range outdoor radiocommunication systems and radio local area networks in the frequency range 300 mhz to 100 ghz," International Telecommunication Union, Tech. Rep. P.1411-9, 2019.

[34] I. T. U. (ITU), "Specific attenuation model for rain for use in prediction methods," International Telecommunication Union, ITU-R Recommendation P.838-3, 2005.

[35] M. J. Miller, B. Vucetic, and L. Berry, *Satellite Communications: Mobile and Fixed Services* (The Springer International Series in Engineering and Computer Science). Boston, MA, USA: Springer, 1995, vol. 322, ISBN: 978-1-4613-5997-5.

[36] E. Dahlman, S. Parkvall, and J. Skold, *5G NR: The Next Generation Wireless Access Technology*. Academic Press, 2018.

[37] 5G Networks, *5g nr terminologies: Subcarrier spacing, frame, subframe, slot and symbol*, https://www.5g-networks.net/5g-nr-terminologies-subcarrier-spacing-frame-subframe-slot-and-symbol/, Accessed: 2024-01-15, 2024.

[38] International Telecommunication Union, "Radio regulations," International Telecommunication Union, Tech. Rep., 2021, Article 5.391.

[39] 3GPP, "Service requirements for the 5g system (release 18)," 3rd Generation Partnership Project, Technical Specification TS 22.261, version 18.1.0, 2022. [Online]. Available: https://www.3gpp.org.

[40] T. S. Rappaport, *Wireless Communications: Principles and Practice*, 2nd. Upper Saddle River, NJ, USA: Prentice Hall, 2020.

A

Appendix 1

This appendix provides detailed simulation results for NTN link performance evaluation across multiple environments and frequency bands. All simulations follow 3GPP TR 38.811 standards and consider elevation angles from 10° to 90° to capture the complete range of operational scenarios. The throughput and latency values are calculated using the analytical formulas introduced in Sections 2.5.5 and 2.5.6, while simulation parameters are summarized in Table A.1.

A. Simulation Parameters

Table A.1: Unified Simulation Parameters for S-band and Ka-band Links

Parameter	**S-band** (2 GHz)	**Ka-band** (20 GHz)
Carrier Frequency	2 GHz	20 GHz
Bandwidth	2 MHz	10 MHz
EIRP	43 dBW	65 dBW
UE Antenna Gain	12 dBi	25 dBi
Noise Figure	2 dB	1.5 dB
Noise Temperature	290 K	290 K
Satellite Altitude	600 km	600 km
UE Speed	120 km h^{-1}	120 km h^{-1}
Modulation Scheme	QPSK	QPSK
OFDM Subcarriers	64	64
Cyclic Prefix Length	16	16
OFDM Symbols	100	100
Monte Carlo Trials	10^6	10^6

B. Free Space Path Loss (FSPL) Baseline

Table A.2: Free Space Path Loss Baseline Performance

Elev. [°]	**Path Loss** [dB]		**CNR** [dB]		**Throughput** [Mbit s^{-1}]	
	S-band	**Ka-band**	**S-band**	**Ka-band**	**S-band**	**Ka-band**
10	164.19	184.19	31.29	32.20	3.27	16.36
30	159.10	179.10	36.71	42.02	3.27	16.36
50	156.10	176.10	39.77	45.92	3.27	16.36
70	154.52	174.52	41.37	47.85	3.27	16.36
90	154.03	174.03	41.86	48.44	3.27	16.36

C. Rural Environment Results

Table A.3: Rural Environment Performance with Shadow Fading and Clutter Loss

Elev. [°]	**CNR** [dB]		**BER**		**Throughput** [Mbit s^{-1}]	
	S-band	**Ka-band**	**S-band**	**Ka-band**	**S-band**	**Ka-band**
10	-6.52	-15.01	0.354	0.440	2.12	9.16
30	4.81	1.82	0.083	0.150	3.00	13.91
50	9.87	8.92	6.67×10^{-3}	9.43×10^{-3}	3.25	16.21
70	13.07	11.95	1.75×10^{-4}	4.36×10^{-4}	3.27	16.36
90	15.16	14.94	2.81×10^{-6}	1.43×10^{-6}	3.27	16.36

- **S-band reliability**: Positive CNR maintained down to 30° elevation, while Ka-band becomes marginal.
- **High-elevation advantage**: Both bands achieve excellent performance (BER $< 10^{-6}$) at 90° elevation.
- **Throughput**: Ka-band delivers $\approx 5\times$ higher throughput but is more sensitive to elevation.
- **Environmental penalty**: Additional 26 dB–47 dB loss compared to FSPL baseline.

D. Urban Environment Results

Table A.4: Urban Environment Performance

Elev. [°]	**CNR** [dB]		**BER**		**Throughput** [Mbit s^{-1}]	
	S-band	**Ka-band**	**S-band**	**Ka-band**	**S-band**	**Ka-band**
10	-10.32	-18.81	0.404	0.461	1.95	8.81
30	1.01	-1.98	0.186	0.252	2.66	12.25
50	6.07	5.12	0.055	0.065	3.09	15.30
70	9.26	8.15	0.011	0.016	3.24	16.11
90	11.36	11.14	1.66×10^{-3}	1.21×10^{-3}	3.27	16.34

- **Degradation**: Additional 4 dB–6 dB loss compared to rural environment.
- **Operational threshold**: Reliable operation (BER $< 10^{-3}$) only achievable above 70° elevation.
- **Throughput impact**: Significant degradation at low elevations.
- **Frequency neutrality**: Both bands show similar degradation patterns.

E. Dense Urban Environment Results

Table A.5: Dense Urban Environment Performance

Elev. [°]	**CNR** [dB]		**BER**		**Throughput** [Mbit s^{-1}]	
	S-band	**Ka-band**	**S-band**	**Ka-band**	**S-band**	**Ka-band**
10	-14.22	-22.71	0.438	0.475	1.84	8.59
30	-2.89	-5.88	0.284	0.335	2.34	10.89
50	2.17	1.22	0.154	0.167	2.77	13.64
70	5.36	4.25	0.070	0.085	3.04	14.97
90	7.46	7.24	0.030	0.027	3.17	15.93

- **Severe challenges**: Additional 8 dB–10 dB loss compared to urban environment.
- **Usability limits**: Even at 90°, BER remains $\approx 3 \times 10^{-2}$ (unacceptable for mission-critical links).
- **Throughput constraint**: Reduced to 3.17 Mbit s^{-1} (S-band) and 15.93 Mbit s^{-1} (Ka-band).
- **System implications**: Requires diversity, coding, or hybrid satellite-terrestrial solutions.

F. Comparative Analysis Summary

Table A.6: Performance Summary Across Environments

Environment	Additional Loss vs FSPL [dB]	Min. Elev. for BER $< 10^{-3}$ [°]	Max. Throughput [Mbit s^{-1}]	
			S-band	Ka-band
Free Space	0	All	3.27	16.36
Rural	27–47	50	3.27	16.36
Urban	31–53	70	3.27	16.34
Dense Urban	35–57	>90	3.17	15.93

G. Monte Carlo Simulation for BER Estimation

To evaluate BER under realistic noise and channel impairments, a Monte Carlo simulation was conducted using OFDM with QPSK modulation. For each trial, random bits were generated, modulated, passed through an AWGN channel (SNR-based), demodulated, and compared with the transmitted sequence. The BER is computed as:

$$\text{BER} = \frac{\text{Number of Error Bits}}{\text{Total Transmitted Bits}}$$

The process repeats for 10^6 trials to ensure statistical stability.

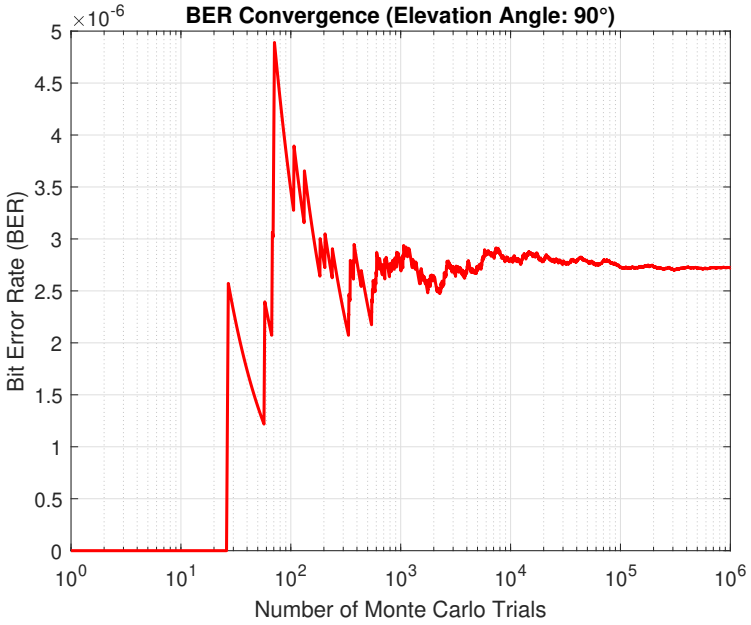

Figure A.1: BER convergence over Monte Carlo trials.

Observation: The convergence curve confirms that the chosen trial count ensures reliable BER estimation with minimal statistical fluctuation.

H. Doppler Shift Analysis for High-Speed Terminals at Different Altitudes

Figures A.2–A.5 present Doppler shift variations for a user terminal moving at 1000 km h^{-1} under three mobility cases: stationary, moving toward, and moving away from the satellite. Altitudes of 600 km, 1500 km, and 10.000 km are considered for both 2 GHz and 20 GHz.

Key observations:

- Higher altitudes reduce Doppler shift magnitude due to lower relative angular velocity of the satellite.
- At 20 GHz, Doppler shifts are ≈10× higher than at 2 GHz, increasing the need for precise frequency tracking.
- Doppler passes through zero at zenith (mid-pass), with maximum positive/negative shifts near the horizon.

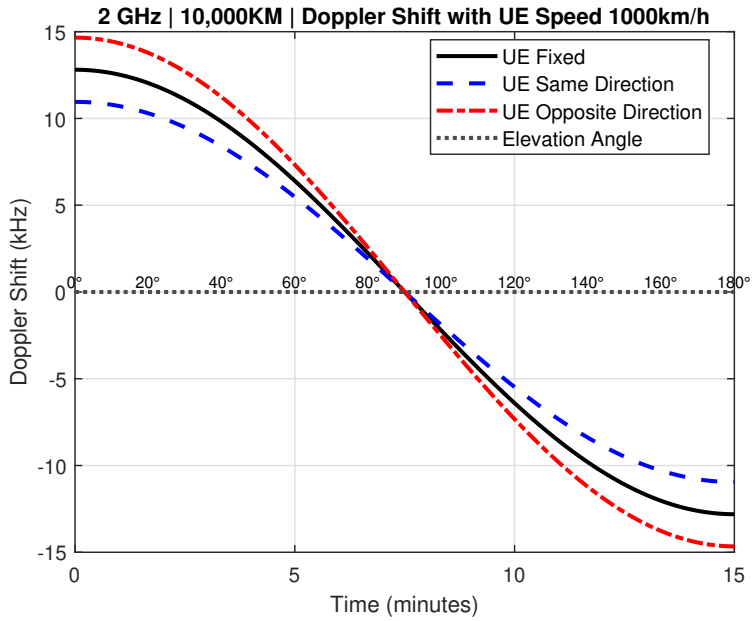

Figure A.2: Doppler shift at 10.000 km altitude for 2 GHz

Observation: Doppler remains at ±14.6 kHz*, relatively easy to compensate with standard AFC techniques.*

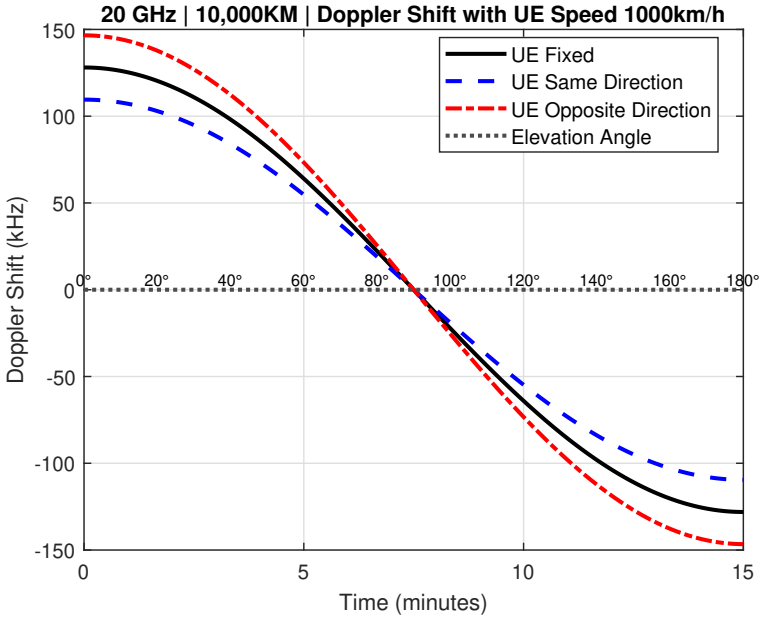

Figure A.3: Doppler shift at 10.000 km altitude for 20 GHz

Observation: Peak shifts approach ±146.5 kHz*, requiring robust Doppler compensation algorithms.*

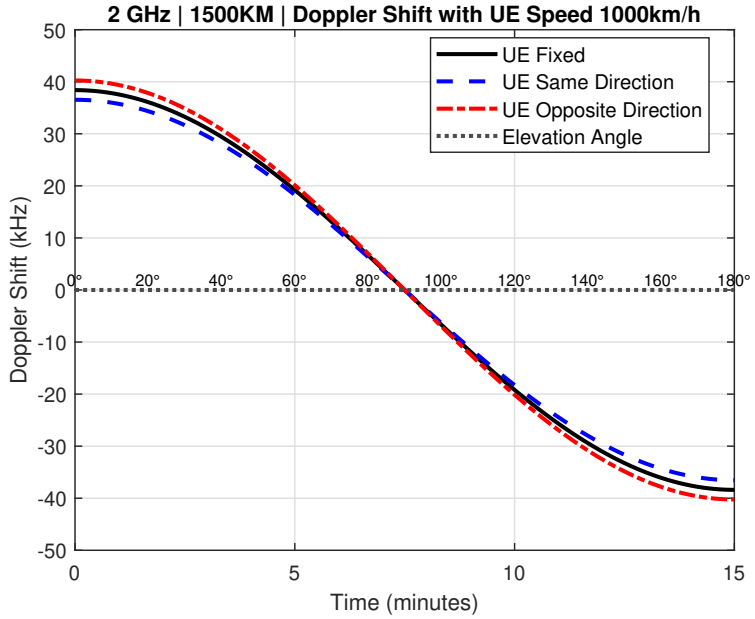

Figure A.4: Doppler shift at 1500 km altitude for 2 GHz

Observation: Doppler peaks at ±40.2 kHz*, manageable for narrowband systems but potentially problematic for wideband links without correction.*

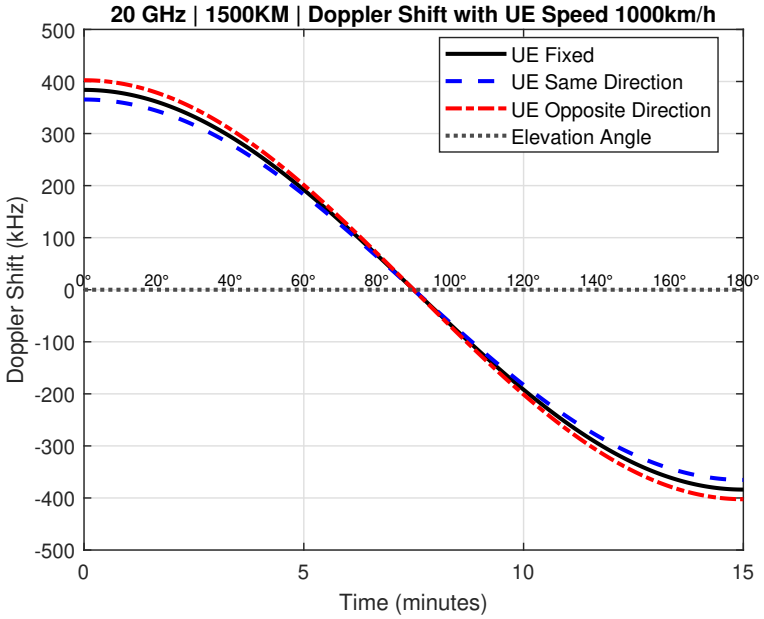

Figure A.5: Doppler shift at 1500 km altitude for 20 GHz

Observation: Peaks at ±402 kHz, making Doppler pre-compensation or adaptive equalization essential for reliable demodulation.

B

Appendix 2

This appendix provides an overview of the simulation framework and key algorithms implemented in MATLAB for evaluating NTN link performance. The code follows a modular structure with clear separation of physical layer components.

A. Main Simulation Workflow

```
function main_code()

    % --- System Parameters ---
    params = getNTNSimulationParameters('s-band');
    elevationAngles = [10,30,50,70,90];
    scenario = 'rural';
    dopplerDirection = 'away';

    % --- Result Storage ---
    results = initializeResultsTable(elevationAngles);
    berConvergenceAll = zeros(params.numTrials, length(
       elevationAngles));

    % --- Loop over elevation angles ---
    for i = 1:length(elevationAngles)
        elevationAngle = elevationAngles(i);

        % --- Channel Effects ---
        dopplerShift   = computeDopplerShift(...);
        distance       = calculateDistance(...);
        FSPL           = calculateFSPL(...);
        [CL_dB, SF_dB] = largescalemodel(...);
        atmosphericLoss= calculateP618Losses(...);

        % --- Link Analysis ---
        [ber, throughputDL, CNR, SNR, berConv] = simulation
           (...);

        % --- Latency ---
        totalLatency = calculateLatency(distance);

```

```
30          % --- Store Results ---
31          results = updateResults(...);
32          berConvergenceAll(:, i) = berConv;
33      end
34
35      % --- Output & Plots ---
36      displayResults(results);
37      plotResults(results, berConvergenceAll, ...
38                  elevationAngles, params.numTrials);
39
40  end
```

Listing B.1: Main simulation code workflow.

The overall workflow of the simulation is summarized in Listing B.1. At the beginning of the execution, the function `getNTNSimulationParameters` is used to configure the system parameters. This function allows the selection of different frequency bands, such as S-band or Ka-band, and provides the corresponding carrier frequency, bandwidth, satellite transmit power, antenna gains, and other link budget parameters. The main code then defines the simulation conditions, including the propagation scenario (e.g., rural, urban, or dense urban) and the Doppler direction (either *away*, *toward*, or *fixed*).

For each elevation angle, the channel impairments are calculated, including Doppler shift, slant range distance, free-space path loss, clutter loss, shadow fading, and atmospheric attenuation based on ITU-R P.618 models. These values are then passed to a link-level simulator that computes the bit error rate (BER), achievable downlink throughput, carrier-to-noise ratio (CNR), and signal-to-noise ratio (SNR). Latency is determined as a function of propagation delay derived from the satellite slant range. Finally, the computed metrics are stored in tabular form, convergence of BER across Monte Carlo trials is recorded, and the results are visualized through dedicated plots.